TÉCNICO LISBOA

An integrated FSI analysis of a windsurfer fin

Miguel Afonso Cardoso de Brito

Thesis to obtain the Master of Science Degree in

Aerospace Engineering

Supervisors: Prof. José Manuel da Silva Chaves Ribeiro Pereira
Dr. Leigh Stuart Sutherland

Examination Committee

Chairperson: Prof. Filipe Szolnoky Ramos Pinto Cunha
Supervisor: Dr. Leigh Stuart Sutherland
Member of the Committee: Prof. André Calado Marta

April 2021

”It always seems impossible until it’s done”

Nelson Mandela

Acknowledgments

This thesis marks the end of a five year journey through IST, which was defined by many people whom I would like to thank.

First and foremost, I would like to thank both of my advisors Prof. José Chaves Pereira and Dr. Leigh Sutherland, for the support during this project. Dr. Leigh was always available at the other end of an e-mail, helping to guide me along this thesis with his experience and knowledge. His expertise in the field of composites and naval engineering was crucial to the development of this thesis. Prof. José help was fundamental for the development and understanding of the CFD simulations, and the multiple zoom calls that we had were always instructive and I always felt like I learned something new. Thank you to both of you.

I would like to thank Eng. Mário Arruda for his help in developing the ABAQUS FEA model, I could always contact him with any problem regarding the software.

I would also like to thank Duarte Albuquerque for his help navigating the problems with LASEF computers, which ultimately allowed me to run all the simulations.

To all of my friends, in and out of university, with whom I had many adventures. This period would be nothing without those memories.

Finally, to all of my family who helped me along the way, supporting me throughout this journey.

To all of you, thank you.

Resumo

Este trabalho consiste no desenvolvimento de uma ferramenta para investigar o comportamento de uma quilha de windsurf, produzida em materiais compósitos, em movimento na água.

O projeto pode ser dividido em três partes fundamentais. (i) O desenvolvimento de um modelo estrutural (FEA), em ABAQUS, para estudar a resposta do material compósito às cargas aplicadas na quilha, incluindo uma melhoria signficativa da estimativa das propriedades dos materiais. (ii) O desenvolvimento de um modelo hidrodinâmico (CFD), em Star-CCM+, que analisa o comportamento do fluido envolvente e os campos de pressão criados pela presença da estrutura. (iii) O acoplamento dos dois modelos mencionados, para a criação de um modelo de Interação Fluido-Estrutura (FSI).

Um estudo paramétrico foi feito, usando a ferramenta, para diferentes situações de navegação, com uma gama de velocidades de 10 a 35 nós e ângulos de ataque de 2 a 8 graus. Os resultados deste estudo ajudaram a compreender melhor três respostas principais: a força de sustentaçao na superfície da quilha, a defleção na ponta da quilha e o ângulo de torção. Os resultados mostraram que tanto a força de sustentaçao como a deflexão da quilha aumentaram tanto com a velocidade como com o ângulo de ataque. Observou-se também que o ângulo de torção é um parâmetro muito sensível à alterações no escoamento. Um estudo sobre a necessidade do uso do modelo de múltiplas iterações também foi feito e os resultados comparados com o modelo simples de FSI. Finalmente, a situação de perda foi estudada, analisando o comportamento da quilha num ângulo de ataque de 8 graus.

Um melhor conhecimento do comportamento estrutural da quilha foi conseguido como consequência desta Tese. Este projeto resultou também no desenvolvimento de uma ferramenta que permite fazer estudos paramétricos em quilhas, podendo-se alterar a composição dos compósitos, a sua orientação, a velocidade do fluido e o ângulo de ataque da quilha.

Palavras-chave: FSI, CFD, FEA, ABAQUS, Star-CCM+,Materiais Compósitos, Quilha de Windsurf

Abstract

This work consists of the development of a design tool that allows the user to investigate the behaviour of a windsurf fin, made of composite materials, in motion.

This project can be divided in three main sections. (i) The development of a completely new structural model (FEA), in ABAQUS, to study the response of the composite material to the loads applied at the fin, including a comprehensive research on the material's properties. (ii) The development of a hydrodynamic model (CFD), in Star-CCM+, which analyses the behaviour of the surrounding fluid and the pressure fields generated by the fluid on the fin. (iii) The coupling of these two models, to create a fluid-structure interaction (FSI) model.

A parametric analysis then both commissioned this tool and provided initial results to different operating conditions, with velocities ranging from 10 to 35 knots and angles of attack from 2 to 8 degrees. Results obtained from this study helped understand three main structural responses: lift force on the fin's surface, fin tip deflection and tip twist. It was found that both the lift force and the tip deflection of the fin increased with both velocity and angle of attack. The angle of twist was found to be very sensitive to changes in the flow. Further, the situations where the additional resources required for the two-way FSI could be safely avoided by using a simpler one-way model were identified. Finally, the stall condition was studied, analysing the behaviour of the fin at an angle of attack of 8 degrees.

This thesis marks an improvement of the knowledge of the structural behaviour of the fin under operating conditions. Also, the developed design tool facilitates the study of fins with respect to parameters such as the composite materials composition, its orientation, fluid velocity and angle of attack.

Keywords: FSI, CFD, FEA, ABAQUS, Star-CCM+, Composite Materials, Windsurf Fin

Contents

List of Tables

List of Figures

Nomenclature

Greek Symbols

α or AoA	Angle of attack
δ_e^T	Internal strains
E	External virtual work
I	Internal virtual work
ϵ	Strain tensor
η_0	Correction for the non-unidirectional reinforcement
η_L	Length Correction Factor
ν_c	Poisson's Ratio of composite
ν_f	Poisson's Ratio of fibre
ν_f	Poisson's Ratio of matrix
ρ	Density
ρ_c	Density of Composite
ρ_f	Density of Fibre
ρ_m	Density of Matrix
σ	Stress tensor
σ^T	Internal stresses

Roman Symbols

A_c	Area of Composite
C_D	Drag Coefficient
C_L	Lift Coefficient
C_p	Pressure Coefficient
D	Drag Force
E_m	Young's Modulus of fibre
E_m	Young's Modulus of matrix
E_{cL}	Longitudinal Young's Modulus of composite
E_{cT}	Transverse Young's Modulus of composite
E_c	Young's Modulus of short fibre composites
E_{fL}	Longitudinal Young's Modulus of fibre
E_{fT}	Transverse Young's Modulus of fibre
f^T	Forces per unit volume
FVF	Fibre Volume Fraction
FWF	Fibre Weight Fraction
G_{cLT}	Longitudinal Transversal Shear Modulus
G_f	Shear Modulus of fibre
G_m	Shear Modulus of matrix
L	Lift Force
L/D	Lift to Drag ratio
m_c	Mass of Composite
m_f	Mass of Fibre
m_m	Mass of Matrix
S	Wing Area
t	Thickness
t^T	Forces per unit area

V_∞	Free Stream	v_m	Volume of Matrix
v_c	Volume of Composite		
v_f	Volume of Fibre	W_F	Fibre area weight

Glossary

2D Two-Dimensional. 17, 41

3D Three-Dimensional. 15, 16, 22, 32

ALE Arbitrary Lagrangian Eulerian method. 40

CAD Computer-Aided Design. 22, 23, 32

CFD Computational Fluid Dynamics. 1, 6, 22, 31, 41

FEA Finite Element Analysis. 6, 11, 22, 31, 42

FEM Finite Element Method. 1

FRC Fibre Reinforced Composite. 3, 10, 11

FSI Fluid Structure Interaction. 2, 5, 6, 34, 39, 46

IST Instituto Superior Técnico. 5, 32

LASEF Laboratory and Simulation in Energy and Fluids. 32

VOR Volume of Refinement. 33

Chapter 1

Introduction

The sport of windsurfing, as we know it today, has been around since the 1970's. Emerging from the surf culture of California, it is a combination between surfing and sailing.

Newman Darby is credited for the conceptualization of the sport. Sailboats were already in use for centuries, and Darby with the idea of simplifying and doing an adaptation of a sailboat, in 1948 assembled a hand-held sail to a universal joint, fixed to a floating board calling it sailboarding. The sailboard is nowadays known as windsurfer.

This simple invention spread all over the world and gained a lot of supporters, with the enormous popularity of the sport in the late 1970's leading to it being a demonstration sport in the 1984 Olympic games. After a short decline in popularity in the 1990's, the sport has had a revival in the 2000's. Nowadays it is used mainly for leisure and competitive purposes with the competitive aspect growing a lot in recent years, being one of the sailing events on the Olympic Games in Tokyo 2021, the RS:X [1]. This increase in competitiveness has been observed by designers and manufacturers of windsurf equipment, hence large efforts have been made to design and create the best windsurf equipment to suit the requirements of each rider. In order to do this, manufacturers ally themselves with engineering knowledge to produce the best gear possible.

1.1 Motivation

The aspiration for a better design of the windsurf fin, one which takes into account the influence of the fluid on the structure and of the response of the structure in the fluid domain, is what led to the existence of this Thesis.

With the improvement of technology, specifically engineering softwares, it is now possible, through computational analysis, to take into account both aspects of the design of a fin simultaneously. These technologies include Finite Element Method (FEM) analysis to study the structural behaviour of complex and, in this case, anisotropic structures. The use of Computational Fluid Dynamics (CFD), which allows a trustworthy analysis of the fluid around the structure, as well as the ability to calculate the load exerted on the structure by the moving fluid. Finally, joining both of these simulations, we will arrive to a Fluid-

Structure Interaction (FSI) problem, where both softwares will communicate with each other, sharing fields in order to arrive at a final solution.

Classical studies are often only one-way analysis, that do not consider the deflection of the fin due to the fluid forces. However, windsurf fins are known to have high deflection, therefore a study of the influence of FSI simulations will be done. This study will inform about the effect of the FSI on the results, as well as, which operating conditions results vary more with or without the FSI.

The fin of a windsurfing board is a very important component of the board, as it is mainly responsible for counterbalancing the sail side lift. Similarly to a wing on an airplane being the main source of lift. In figure 1.1, it is clear one of the main responsibilities of the fin, countering the aerodynamic side force of the sail with its own hydrodynamic side force. In the case of the windsurf fin, contrarily to the case of airplane wings, the lift is mostly horizontal, only having vertical components due to the deflection of the fin. This happens because an airplane wing is horizontal to the incoming fluid, while the fin is vertical.

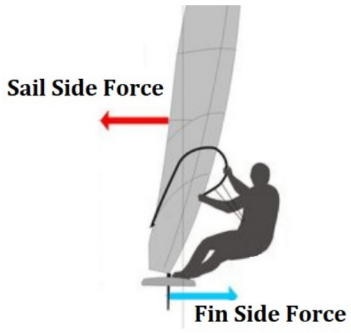

Figure 1.1: Windsurf system balancing side forces

When sailing, the fin is usually not parallel to the incoming flow, it appears to be side slipping. This side-slip phenomenon occurs because the heading of the board does not correspond to the course of sailing. The course direction corresponds to the incoming flow direction seen from the windsurf board while the heading is the direction to which the board is pointed towards. The difference between these two directions is called the “leeway” angle and is the angle of attack at the fin, which, because it has the cross-sectional shape of an aerofoil, is responsible for the appearance of hydrodynamic forces that will balance with the aerodynamic forces of the windsurf sail. A schematic view of the mentioned concepts is presented in figure 1.2.

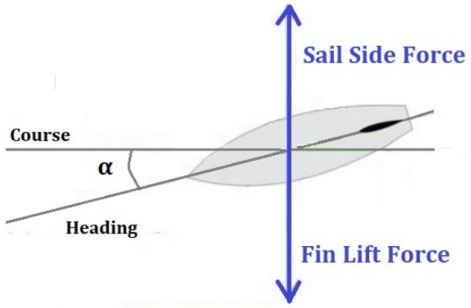

Figure 1.2: Difference between course and heading direction

1.2 State of the Art

1.2.1 Composites in the maritime industry

Fibre reinforced composites (FRC) have been successfully used in maritime applications since the 1940's, originally only used in small crafts, they have since evolved to being part of key components in everything from sailboards to super yachts. Not only have these composites been used in different kinds of boats, but with new purposes such as bearings, propellers or even pipes [1].

The first records of FRC materials being used in maritime applications date back to the World War II, 1947, when boat builders started replacing old materials like plain wood due to its scarcity and price [2].

Following that period of time, the use of FRC materials spread into surfing, surfboards started to be manufactured with these composites due to its weight advantage, which is of paramount importance in a competitive sport. Nautical sports soon began to make the transition to FRC, mainly using fibreglass, resin and a foam core as the materials for the builds. Simultaneously, the oil and gas industry began to use these materials, due to its fire and blast resistant capacities, on protection equipment and pressure vessels [3].

Nowadays, it is common to see sailing boats and nautical sports be at the forefront of new composite technology and materials. Lightness, strength, durability and precise production makes composite materials the most convenient choice in not only the maritime industry but the aeronautical industry as well. With the windsurfing fin being one of the perfect examples of its value.

Windsurfing is quite a new sport, relatively, so, it makes sense, that early in its life composite materials were adopted. Boards, fins and various rigging parts are under constant development, with the sport evolving at a staggering rate and world records being broken every year. Fins are crucial for the performance of a windsurfing rig, they resist to the side force generated by the wind and are one of the main contributors to the velocity, control and manoeuvrability. Carbon fibre fins have a better performance, despite the higher price tag, delivering a more reliable lift while being stiff and are generally low twist structures which are often preferred.

The search for development in the design and production of fins and boards led not only to the adoption of composite materials but also, to the development of new shapes and new internal structures. The design of the fin is so important to its performance, that different fins are used for each specific purpose, especially in competition. The most used fins are: Race Fins, Free-Ride Fins, Wave Fins and Slalom Fins; each having different characteristics that allow for better performance in its situation. Designers can change parameters like length, width, profile, material and its internal structure.

The fin that will be studied in the present work is a slalom Fin produced by F-Hot [4], some examples are presented in figure 1.3. The slalom fins tend to be longer and slender, providing a good ratio of lift to drag and are very versatile, which allow the rider to sail in different conditions and speeds without getting stall due to flow separation.

Figure 1.3: Slalom fins from F-Hot [4]

1.2.2 Windsurf hydrodynamics

Plenty of studies from aerodynamics and similar subjects can be easily applicable to this study, this is not an expansive section. Instead focusing on a few works, closely related with windsurfing specifically.

The flow around a windsurf fin, similarly to the flow around an airplane wing, is governed by the geometric shape, the orientation and speed compared to the flow, as well as other flow parameters such as depth of immersion, viscosity and density [5]. Many of these factors can make it extremely difficult to predict flow conditions and, therefore, predict the fin response, however the fin will be studied under normal conditions.

If a streamlined shape is considered, the nature of the flow can be predicted through experimental techniques, reference to empirical data or computational simulations. As the fin behaves as a wing, empirical data available from the aeronautical industry will be used, as wings have been thoroughly investigated [6]. Since the fin acts as a lifting surface, although positioned vertically instead of horizontally, the classical lifting theory can be used to investigate the fluid around the fin. Computational Fluid Dynamics complement both experimental and empirical approaches, and help understand the results of the theory while still not being able to replace the other methods [7].

Previous research around this topic was made in the University of Exeter and Southampton [8], in the United Kingdom, in 1992, where the effect of platforms and surface finishes of fins on the performance and manoeuvrability of a sailboard was investigated. Uncovering fluid dynamics involved in the design of fins. Afterwards, the effect of the tip flexibility on the performance of a new windsurf fin was also investigated [9]. This fin was better than other fins, especially for high-speed windsurfing and it was found that a slight increase in tip flexibility resulted in higher performance comparatively to using rigid tips.

Two researchers from the University of Bournemouth investigated if changing the geometric cross-sectional shape to one with camber, would lead to an increase of lift on the windsurf fin [10]. Fins on a windsurf board must be able to operate on both directions, or tacks, and because of that a symmetrical cross-section is often used. However, this has the drawback of limiting the amount of lift that the fin

is able to generate in a given angle. In this paper, it was shown that the symmetrical cross-section has a lift coefficient with a low ceiling, while the camber can increase this value while maintaining the same thickness to chord ratio. The camber solution has better lift coefficient for a range of angles of attack, while also decreasing the drag coefficient, making it a superior design for some angles of attack. However, this solution has the obvious drawback that it is optimal for one angle of attack, while windsurf fins will operate in very different conditions. The solution to overcome this problem is to use variable fins with mechanically hinged leading or trailing edges, a resource used often in the aeronautical field. This solution was tested afterwards, with one of the researchers coming up with a design solution which consisted of a hinged deck mechanism on the board which would activate flaps on the fin, generating camber [11].

In a more recent paper, from 2007 [12], the maximum velocity of a windsurfer was studied through modelling of the movement of the rider over a finite number of sails with a prescribed shape, with many environmental variables taken into account. The conclusions showed that a larger sail would turn into higher velocities, however the windsurfer needs to be able to withstand the sail with his hands and body weight, in addition the fin will also have to resist the high hydrodynamic loading.

Finally, the concept of passively tailoring composite materials has recently been applied to high performance sailing boat lifting foils. A study from 2008 investigated sailing styles and boat set-ups, in particular the fore-aft position of the helm and how this could be combined with the aft foil to maximise speed. [13]. More recently, a study on the dynamic fluid-structure interaction of C-foils was done [14]. These foils, often used in off-shore trimarans and adapted to high speed catamarans, not only give the right amount of horizontal side force, but also, deliver a vertical force that can support most of the mass of the boat. Lastly, a study on the fluid-structure interaction of passive adaptive composite foils was done, in 2017 [15]. This studied the influence of adding bend-twist coupling oriented plies to hydrofoil structures. Resulting in an increase of the control over the achievable twist compared with the initial design.

1.3 Objectives

This work arises with the intention of complementing a sequence of several other recent studies that have been developed in IST concerning the analysis of a Windsurf Fin.

The topic was addressed in 1993 by Sutherland [16], and since then the author has manifested the interest of further investigating the subject, ultimately getting to a rigorous and close to reality analysis of the behaviour of the Windsurf Fin when in operation. Related works have been made more recently by Nascimento [17], who focused on the study of the structural simulation of this windsurf fin through Finite Element Model analyses using ANSYS. This study was then further explored by Balzer [18]. Regarding the hydrodynamic aspect of the project, a study by Santos [19] that focused on the analysis of the fluid flow around the same windsurf fin, gives attention to the obtainment of the hydrodynamic loads on the fin. Finally, a study from Saldanha [20] who focused on the hydrodynamic and FSI analysis, without being able to fully autonomize the process due to complications. All these studies done have proven

to be significant steps towards a final and meticulous study of the windsurf fin. The present Thesis will contribute as one of the final steps of this continuous work that has been developed for the past several years.

The main objective set for this thesis is to develop a design tool to evaluate a windsurf fin, which allows for the composition of the fin to be easily interchangeable and ultimately to improve the internal architecture of a windsurf fin. It will also be applicable to other cutting-edge applications of composite foils, such as hydrofoils, aircraft wings and wind and tidal turbine blades. In order to develop this tool, there is the necessity to build both a structural and an hydrodynamic model, which will be combined in a fluid-structure interaction analysis to arrive to the best design possible.

The development of this design tool will be separated into different phases, beginning with the development of the finite element analysis model, from scratch, in ABAQUS, in which the structural composition of the fin will be analysed and validated against an experimental procedure. In order to have a precise FEA model, the material properties estimation has to be greatly improved.

Subsequently, a computational fluid dynamics model will be developed, where the flow around the fin will be analysed and from which pressure fields will be originated.

Finally, the fluid-structure interaction model will be completed, joining the two models previously mentioned and arriving to the final design tool, which will then be used in a parametric study. This study will analyse the influence of the velocity and angle of attack, on three main outputs: the fin's tip deflection; lift force acting on the surface of the fin; and the fin's tip twist. The FSI study will also be compared with a one-way coupling, to see how much influence the two-way coupling has on the final results, as well as, which operating conditions are the most affected.

1.4 Thesis Outline

The thesis structure is divided into 7 main sections.

The first chapter is an introduction to the work done, presenting the need for this work to be done, given the current literature state, as well as a brief explanation of the physics of the windsurf problem.

The second chapter presents the theoretical background needed to understand and develop this thesis. It presents the extensive research done on material properties, the reasoning behind all the choices made in the softwares utilized and a description of the fin at study.

The third chapter explains the development from scratch of the structural model, reviewing the overall process needed to develop the FEA model, this is the first step of the development of the design tool.

In chapter four, the CFD model is presented, the process of developing a model of this type is well defined and its most prominent features are explained. This is the second step on the development of the FSI model.

The conclusion of the model development is on chapter five, where the FSI coupling is explained. Here, similarly to chapter three and four, the process of developing this model is presented. Special consideration goes into the coupling between both CFD and FEA softwares.

Chapter six presents the results of a parametric study. The results of the three outputs, the lift

force on the fin's surface, the fin's tip deflection and tip twist are analysed and physical, engineering explanations are found for each result. A operating condition where stall is expected is also analysed, in order to verify the performance of the design tool.

Finally, chapter seven is a conclusion of this work, showing the achievements of this project, as well as referring to possible future work on this design tool, both to improve it and to use the tool in order to improve fin design.

Chapter 2

Background

2.1 Composite materials concepts

Composite materials are composed by two or more elements, which remain distinct, that are combined to produce a new material that has different properties from both constituents. Most composites used are made of a binding agent, called matrix, and reinforcements, the fibres. The combination of both components is made taking into account the desired final properties and behaviour of the material for a specific application. The application of the materials, lamination, can be made at different angles that allow the designer to tailor the properties in the different directions, taking advantage of the anisotropic behaviour of the composites, for example orienting materials towards highest loadings.

The biggest advantage in using a composite material is the fact that it combines the good characteristics of both the resin and the fibres, which results in materials that can be very light and, at the same time easily formed into complex structures. The resin matrix spreads the load applied to the composite between each of the individual fibres and also protects the fibres from damage caused by abrasion and impact.[21] As can be seen in figure 2.1, the matrix has a predominantly plastic behaviour, while the fibre has a solely elastic behaviour. Combining these two materials, the resulting composite has a blend of both characteristics.

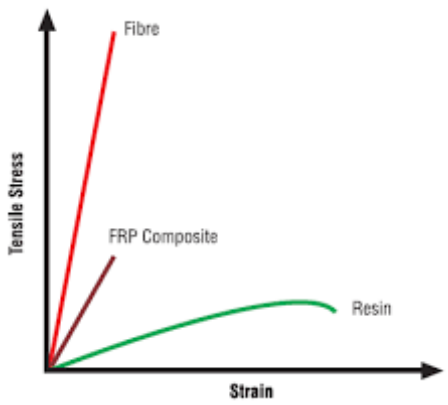

Figure 2.1: Generic stress-strain of fibre, resin and the final composite [21]

The properties of the composite material are dependent on multiple factors: the properties of both components, resin and fibres; the ratio between fibre and resin; and lastly the geometry and orientation of the fibres [21]. As can be seen in figure 2.2, the fibres can be placed in many different orientations, which will alter their performance against similar strains.

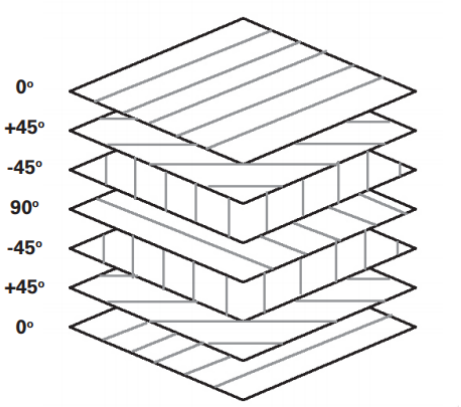

Figure 2.2: Fibers orientation [21]

There are many different kinds of composites, however the most common composite material used for maritime purposes and the composite used in the fin at study, is a Fibre Reinforced Composite (FRC). This material has multiple benefits when compared with other, more common, materials such as, steel, aluminium or wood. Among these benefits it can be mentioned the resistance to corrosion, ease of manufacturing into complex shapes and highly specific material properties [22].

FRC are manufactured through a laminating process, which consists of laying up the fibre layers, embedding them in a resin, the matrix, and molding them into the final geometry. In the case of the fin manufactured by F-Hot, these fibres are then compressed against the mould so that the resin can penetrate through all the different layers and eliminate any existing air bubbles. A small amount of epoxy-fibre cuttings paste is applied in both parts of the fin to fill any potential centre void and both moulds are then bolted together to squeeze out any excess resin.

The matrix used is a bonding agent, usually a polymer liquid that cures to a solid via a chemical reaction, often under vacuum conditions and high temperatures. When combined with the fibre reinforcement, it turns into a stiff material capable of sustaining high loads. In the mould, before plying the fibre layers and the resin, it is applied a material responsible to give a high-quality finish to the visible surface of the composite and, to help with the demolding process, generally a gelcoat is used for this purpose. This is of extreme importance in fin-like products, because the visible surface will be responsible in maintaining the laminar layer, therefore reducing drag.

As mentioned previously, the composite material properties depend heavily on the fibre orientation. which can be of multiple types. In this Thesis the focus will be on Unidirectional (UD) and Woven Roving (WR) fibres.

A UD fabric is one in which the majority of the fibres run in one direction only, a small amount of fibre exists in other directions to support the primary fibres in its positions. UD fibres are straight and uncrimped, which results in the highest possible fibre properties from a fabric in composite component

construction [21]:

- High tensile and compression strengths in the fibre direction, due to the high percentage of fibres in the same direction and also to lack of waviness;
- Low tensile and compression strengths in the crosswise fibre direction [23].

Woven rovings are made from two sets of fibre, warp and weft, criss-crossing at a right angle. Weaving consists in repeating a basic interlace sequence between warp and weft rovings. This sequence is named basic weave and this mechanical interlocking maintains the fabric's integrity. [23]

There are many types of woven roving fibre, in this thesis only plains will be addressed. In plain WR, each weft fibre passes alternatively under and over each warp fibre. WR fibres main characteristics are:

- Fabric is symmetrical, with good stability and reasonable porosity;
- High level of fibre crimp imparts relatively low mechanical properties [21].

The FRC can be composed of many different types of fibres, however as was the case in the orientation, only two main fibre types will be of importance: carbon and glass fibres, specifically E-glass.

Carbon fibres are a high-performance material, its main characteristics are:

- Very high tensile and compression strength and stiffness;
- A very low strength in the normal direction to the fibres' direction;
- Relatively poor interlaminar shear strength and impact resistance [23].

These properties allow for the fin to be stiff without greatly increasing the thickness which would produce more drag. However, carbon is quite expensive therefore glass fibres will be used in the centre where stiffness is not as important. Glass fibres are produced from liquid glass, which are cooled to produce filaments and are available in different forms. Their performance is not as good as carbon fibres, making them popular as a fibre reinforcement. Glass has characteristics such as:

- good tensile and compression strenght and stiffness;
- a relatively poor impact resistance.

2.2 Material Properties

One of the most important steps in developing a FEA model, or any computational model of a real life experiment, is to approximate as closely as possible the experimental data to the one used in the computational simulation. In the FEA case, this translates to material properties.

The FEA material properties need to be the same as in the actual fin, however the fins are hand laminated and then pressure moulded, and not made of pre-preg composites where properties are readily available. Therefore arriving at the final material properties estimation was an iterative process,

not being easy to obtain material properties of an hand crafted structure. These estimations were not obtained by simply fitting the properties to the desired results, these have been verified with other calculation methods and available literature, as well as being based on real properties of other structures.

The initial material properties for the fin were provided by Dr. Sutherland, with help via iterative evaluations of the developing FEA model by the author, with a brief explanation of their derivation given below. For theoretical analysis, volume fractions are of easier use, despite the weight fractions being easier to obtain during the construction and experimental process. In the following equations, the subscripts f, m and c are used to indicate fibre, matrix and composite, respectively. While the letters m and v are used to indicate mass and volume.[3]

The Fibre Weight Fraction (FWF) is easily obtainable during construction simply by weighing the fibre and matrix used, in this study the actual quantities of fibre and resin were used for the estimation, with data from the manufacturer.

$$FWF = \frac{m_f}{m_f + m_m} \tag{2.1}$$

Knowing this relation, the density can be easily established by:

$$m_c = m_f + m_m \tag{2.2a}$$

$$\rho_c v_c = \rho_f v_f + \rho_m v_m \tag{2.2b}$$

$$\rho_c = \rho_f FVF + \rho_m (1 - FVF) \tag{2.2c}$$

$$\rho_c = \frac{1}{(\frac{FWF}{\rho_f}) + (\frac{1-FWF}{\rho_m})} \tag{2.2d}$$

The Fibre Volume Fraction (FVF), which is a very important parameter to tune for the computational model, can be easily obtained by knowing the FWF and the density of both the composite and the fibre.

$$FVF = \frac{\rho_c}{\rho_f} FWF \tag{2.3}$$

One final very important definition for the composite properties is the cured ply thickness. This will give the thickness of each ply taking into account the fibre area weight W_F, the fibre density ρ_f and the FVF for each type of fibre used. This expression was used to define the thickness in the ABAQUS model. A_c represents the area of the composite.

$$\rho_f \cdot FVF = \rho_f \cdot \frac{v_f}{v_c} = \frac{m_f}{v_c} = \frac{m_f}{A_c t} = \frac{W_F}{t} \tag{2.4a}$$

$$W_F = \frac{m_f}{A_c} \tag{2.4b}$$

$$t = \frac{W_F}{\rho_f \cdot FVF} \tag{2.4c}$$

After obtaining all these composite properties, the stiffness of each composite material has to be evaluated by two major parameters, the longitudinal and transverse Young's modulus. At this point, available

library values from ANSYS [24] (subscript 1) for different materials were adjusted for the actual FVF estimates (subscript 2) using a rule of mixtures (ROM) approach [3]. The following equation was used to evaluate the composite longitudinal modulus, where η_0 is 1 for unidirectional fibres and 0.5 for woven roving and η_L is 1 due to the length of the fibres. Equation a) gives the relation between two different FVF's and equation b) gives the final Young's modulus used in the ABAQUS model:

$$E_{cL} = \eta_0 \eta_L E_{fL} FVF + E_m(1 - FVF) \tag{2.5a}$$

$$E_{cL2} = \frac{\eta_0 \eta_L E_{fL} FVF_2 + E_m(1 - FVF_2)}{\eta_0 \eta_L E_{fL} FVF_1 + E_m(1 - FVF_1)} \times E_{cL1} \tag{2.5b}$$

And for the composite transverse Young's modulus:

$$E_{cT} = \frac{E_{fT}}{FVF} + \frac{E_m}{(1 - FVF)} \tag{2.6a}$$

$$E_{cT2} = \frac{\frac{FVF_1}{E_{fT}} + \frac{(1-FVF_1)}{E_m}}{\frac{FVF_2}{E_{fT}} + \frac{(1-FVF_2)}{E_m}} \times E_{cT1} \tag{2.6b}$$

In both equations, (2.5) and (2.6), the L stands for longitudinal, the T for transverse and parameters η_0 and η_L, have to do with fibre length and the orientation of the fibres, respectively [25].

The Young's Modulus of short fibre composites also has to be calculated, which will be important for the definition of the epoxy mixture that fills the left out space inside the fin. This definition, according to Kar [26], is, similarly to the longitudinal one in equation (2.5):

$$E_c = \eta_0 \eta_L E_f FVF + E_m(1 - FVF) \tag{2.7}$$

Here, the main difference to the previous formula is that the η_0 parameter has the value of 0.2, due to the fibres being randomly distributed in the three dimensions [27].

The next material property to evaluate is the Poisson's Ratio (ν), this is a measure of the deformation of a material in directions perpendicular to the direction of loading, which was used to define the material properties in the ABAQUS model. The Poisson's Ratio in all three planes can be calculated by:

$$\nu_{cLT} = \nu_f FVF + \nu_m(1 - FVF) \tag{2.8a}$$

$$\nu_{cLT2} = \frac{\nu_f FVF_2 + \nu_m(1 - FVF_2)}{\nu_f FVF_1 + \nu_m(1 - FVF_1)} \times \nu_{cLT1} \tag{2.8b}$$

Finally, the shear modulus, which is defined as the ratio of shear stress to the shear strain, was also estimated using the ROM equations, presented below, (2.9).

$$G_{cLT2} = \frac{1}{\frac{FVF}{G_f} + \frac{1-FVF}{Gm}} \tag{2.9a}$$

$$G_{cLT2} = \frac{\frac{FVF_1}{G_f} + \frac{1-FVF_1}{Gm}}{\frac{FVF_2}{G_f} + \frac{1-FVF_2}{Gm}} \times G_{cLT1} \tag{2.9b}$$

All the previous values calculated were then verified using a direct Chamis calculation method from the constituent material properties [28]. The values obtained were close to the ROM adjusted values, the latter being used in the study since they came from experimental origins on actual tested laminates, rather than calculated from raw material properties as in the Chamis method. Although the Chamis method is more empirical, ROM values were experimental values adjusted for FVF differences and were, therefore, more accurate.

After taking into consideration all the estimations mentioned, the FEA model was found to be stiffer than the physical experimental test data of the actual fin. From conversations with the manufacturer, it became clear that in the manufacturing process fibres were often curved. This phenomenon usually has two explanations, unavoidable rolling effects and the fitting of the plies into the curved planform mould. Therefore, the longitudinal stiffness will be adjusted due to the effects of fibre-waviness, reducing the composite stiffness. A waviness of 3 mm in each 10 cm of length of the fibre was estimated, following conversations with the manufacturer, resulting in a reduction of the longitudinal stiffness of around 25% for every composite. In figure 2.3 it is shown the correlation between the fibre waviness and the change in Young Modulus [29].

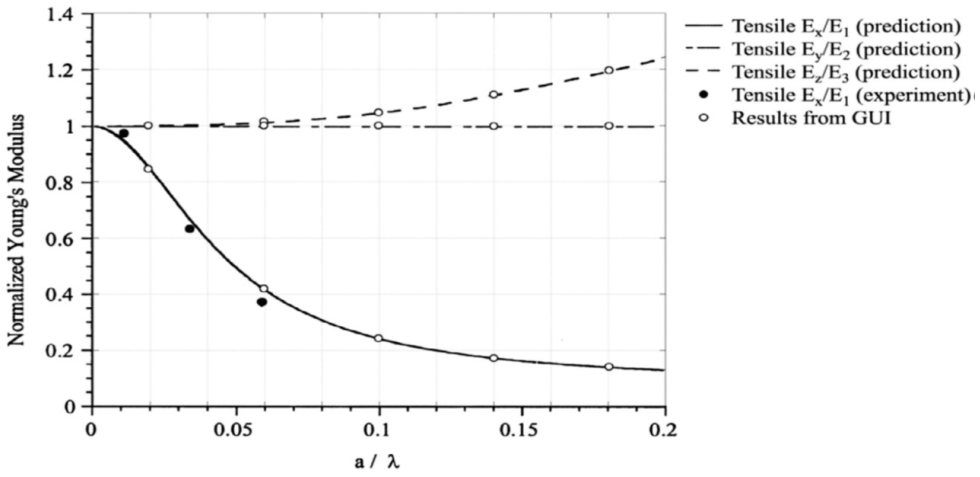

Figure 2.3: Effective stiffnesses in case of uniform waviness. [29]

Further details on the material properties, as well as the final properties used in the FEA model can be found in section 3.3.2.

2.3 Finite Element Analysis

Finite Element Analysis is a numerical method for solving problems of engineering and mathematical physics. It is very useful for problems with complex geometries and material properties, where the analytical solutions cannot be easily calculated, as is the case of the windsurf fin. The goals of the study are to predict the performance and behaviour of the structure, identify any potential breaking points and to calculate safety margins for the design. An optimal design should always be achieved with an iterative project.

The general finite element procedure can be summarized, starting with an arbitrary 3D solid subjected to volume forces per unit volume f^T and surface forces per unit area t^T:

$$f^T = (f_x, f_y, f_z) \tag{2.10a}$$

$$t^T = (t_x, t_y, t_z) \tag{2.10b}$$

Internal stresses and strains can be described as column matrices:

$$\sigma^T = (\sigma_{xx}, \sigma_{yy}, \sigma_{zz}, \sigma_{yz}, \sigma_{xz}, \sigma_{xy}) \tag{2.11a}$$

$$\delta_\epsilon^T = (\delta_{\epsilon xx}, \delta_{\epsilon yy}, \delta_{\epsilon zz}, \delta_{\epsilon yz}, \delta_{\epsilon xz}, \delta_{\epsilon xy}) \tag{2.11b}$$

Following the principle of virtual work, the internal virtual work is [30]:

$$\delta W_I = \int_V \sigma^T \delta_\epsilon dV \tag{2.12}$$

and the external virtual work is:

$$\delta W_E = \int_V f^T \delta_u dV + \int_S t^T \delta_u dS \tag{2.13}$$

The virtual strains are strains that would be produced by virtual displacements $\delta u(x)$. Therefore, virtual strains are computed from virtual displacements using the strain-displacement equations. In matrix notation:

$$\epsilon = \partial u \tag{2.14a}$$

$$\delta_\epsilon = \partial \delta_u \tag{2.14b}$$

Where:

$$\partial = \begin{bmatrix} \frac{\partial}{\partial_x} & 0 & 0 & \frac{\partial}{\partial_y} & 0 & \frac{\partial}{\partial_z} \\ 0 & \frac{\partial}{\partial_y} & 0 & \frac{\partial}{\partial_x} & \frac{\partial}{\partial_z} & 0 \\ 0 & 0 & \frac{\partial}{\partial_z} & 0 & \frac{\partial}{\partial_y} & \frac{\partial}{\partial_x} \end{bmatrix} \tag{2.15}$$

For a linear material, according to Hooke's law [30]:

$$\sigma = E\epsilon \tag{2.16}$$

The internal virtual work over each element becomes

$$\delta W_I^e = \int_{V_e} \sigma^T \delta_\epsilon dV = \int_{V_e} \epsilon^T E \delta_\epsilon dV \tag{2.17}$$

The expansion of the displacements can be written in matrix form as

$$u = Na \tag{2.18}$$

where ”N” contains the element interpolations functions and ”a” the nodal displacements of the element. Therefore the strains are

$$\epsilon = \partial u = \partial N a = Ba \tag{2.19}$$

where $B = \partial N$ is the strain-displacement matrix. Now, the discretized form of the internal virtual work over an element can be computed as

$$\delta W_I^e = a^T K^e \delta a \tag{2.20}$$

where the element stiffness matrix is:

$$K^e = \int_{V_e} B^T E B dV \tag{2.21}$$

Replacing equation (2.21) in equation (2.20), the external virtual work becomes:

$$\delta W_E^e = (\int_{V_e} N^T f dV + \int_{S_e} N^T t dS)\delta_a = (P^e)^T \delta_a \tag{2.22}$$

where the element force vector is:

$$P^e = \int_{V_e} N^T f dV + \int_{S_e} N^T t dS \tag{2.23}$$

The integrals over the element volume V_e and element surface S_e are usually evaluated numerically by the Gauss integration procedure. For the volume integral, such a procedure needs evaluation of the integrand at a few points inside the volume. Such points, which are called Gauss points, are important for two reasons. First, the constitutive matrix E is evaluated at those locations. Second, the most accurate values of strains (and stresses) are obtained at those locations too. Eventually all the element stiffness matrices K^e and element force vectors P^e are assembled into a global system for the whole body [30].

$$Ka = P \tag{2.24}$$

One of the most fundamental steps in developing a sound FEA model is to select which type of elements to use when meshing the geometry. There are many different types of elements in ABAQUS and the choice of elements affects the whole model, since each element requires certain definitions.

2.3.1 Solid elements

The first type of element to be considered was a solid element. 3D solid elements, also known as 3D solid continuum elements, require a 3D mesh which explicitly defines the 3 dimensions of the solid, making this model computationally expensive. It is usually only used in simple geometries due to limitations

with aspect ratio when the thickness direction is very thin when compared with the other two dimensions. They can be used in detailed analysis of specific regions where a rapid variation of stress or strain is expected, since it is possible to transition easily to other types of elements [30] [31].

2.3.2 Conventional shell elements

Conventional shell are general-purpose elements, which provide robust and accurate solutions to most applications, using First-order Shear Deformation Theory (FSDT).

Contrarily to solid elements, conventional shell elements only require the geometry to represent a 2D surface, with the thickness direction being defined through the section property definition. These elements are useful for both thin (S8R5 element type, with 8 nodes) and thick shell (S8R, with 8 nodest) problems and have both displacement and rotational degrees of freedom [30] [31].

2.3.3 Continuum shell elements

Continuum shell elements are elements that are used as solid elements, while using the theory of shell elements, FSDT, to determine the response of the structure. They require the geometry to model explicitly the thickness of the shell, as it would be done with 3D solid elements. Since the thickness is determined from the elemental nodal geometry and these nodes can be stacked, continuum shell elements have the ability to be more precise than conventional shell.

These elements also have drawbacks when compared with the former two. They only have displacement degrees of freedom, the meshing technique is harder than in conventional shell elements and boundary conditions may sometimes be difficult to apply.

Continuum shell elements include linear elements such as SC6R with 6 nodes and SC8R with 8 nodes. [30] [31].

2.4 Bend-twist coupling

Bend-twist coupling is a property of some composite materials, that when subjected to loading conditions that would normally result in pure bending, undergo both bending and twisting [32]. Bend-twist coupling can happen due to three main circumstances: the layup of an anisotropic material; the shape of the structure, for example a swept back fin; and the section shape of the structure.

In the fin studied in this Thesis, the main effect taken into account is the shape of the structure. The fin is a distributed loaded cantilever, which has plies in three directions: 0^o, 90^o and $\pm 45^o$. If the fin was a rectangular cantilever with no errors in the lamination process, there would be no bend-twist as long as the force is applied at the elastic axis. However the fin has a complex shape, with rake aft, which would suggest bend-twist coupling. Also, the laminates are curved into the mould shape as they are laminated, hence the orientation of the plies may be slightly altered when compared with the nominal values. Taking all these details into account, it is uncertain if the fin has bend-twist coupling. The multiple effects could combine to have a null effect, or not, hence, further analysis is necessary to have a concrete response.

Every windsurf discipline has different requirements, therefore there is a specific fin type and shape that bests suits them. Challenging gusty and choppy conditions and wave events need more control and hence, it is beneficial if the bend-twist coupling reduces the angle of attack (washout), in order to avoid stall and reduce load. While steadier flatter conditions and speed or slalom events need no twist or even an increase of the twist for more speed. Controlling the bend-twist coupling effect of the fins could allow to take the best properties out of different designs and combine them all in a better fin with less drawbacks. Normally up to now this has simply been done with changing the fin plan outline. More rake, especially at tip gives washout but is less efficient in terms of L/D, while upright elliptical planform gives speed with high L/D but will stall earlier and faster. Ideally, an upright elliptical fin with internal layup giving bend-twist coupling could have the best characteristics for all conditions. This interaction between bending and twisting, although difficult to master, can be taken advantage of by the designers of composite structures. One of the first examples of this was the swept forward wings of the Grumman X-29, it also is used in wind turbines and is starting to be applied to foil structures [15].

2.5 Hydrodynamic Concepts

2.5.1 Aerofoil

An aerofoil is a curved profile geometry that creates forces as it moves through a fluid flow, due to its shape. It is the cross-sectional shape of airplane wings, helicopter blades, and in the windsurf case of the sail and fin. In the specific case of the fin studied in the present work, the structure is intended to be operated with water as the surrounding fluid, therefore, it is called hydrofoil.

There are some basic concepts of a foil related to its geometry, shown in figure 2.4, that are important to understand when analysing this component. The leading edge, which is usually a rounded edge and the first point of contact with incoming fluid; the trailing edge, which is the sharp edge located at the rear section of the aerofoil; the chord, which is a straight line that connects the leading and trailing edge; the camber line, which is the line that connects the leading and trailing edge of the aerofoil, being equidistant from its upper and lower surfaces; and the thickness of the airfoil, which is the maximum distance between the upper and lower surfaces.

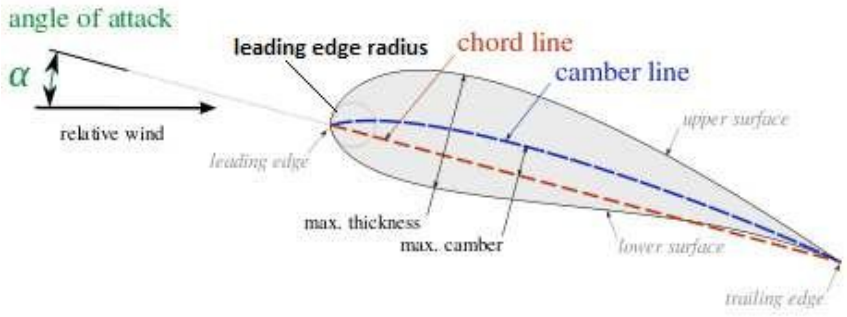

Figure 2.4: Aerofoil Nomenclature [33]

The camber and thickness are two very important parameters when talking about an aerofoil, both

of which are commonly used to define and even give a nomenclature to the foil. The camber influences how much lift the foil is able to generate without an angle of attack. When the camber is null, which translates to the camber line being coincident to the chord line and the foil being symmetric, the foil does not generate lift. This is the case for the Windsurf fin, without an angle of attack or drift angle, the foil will not generate lift as there is no pressure difference between the upper and lower surfaces.

2.5.2 Hydrodynamic Forces

The movement of the hydrofoil through the fluid generates forces, these forces can be decomposed into two components; the lift force, which is perpendicular to the incoming flow; and the drag force, which is parallel to the incoming flow, as can be seen in figure 2.5.

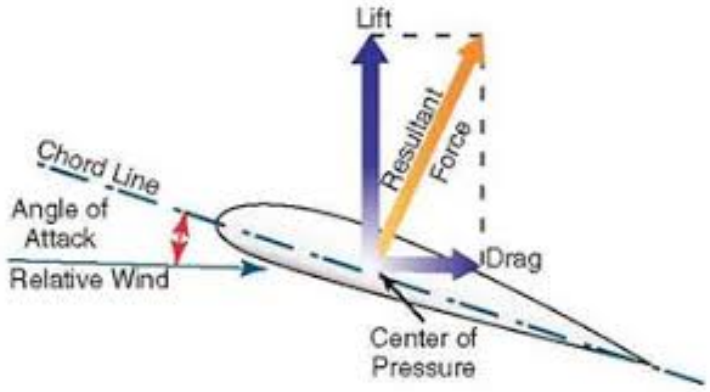

Figure 2.5: Aerodynamic forces on a foil [34]

These forces are generated due to the difference in speed between the upper streamlines and the lower streamlines, which is a direct result of the geometry of the hydrofoil. According to Bernoulli's law, this change in velocity must cause a change in pressure as well, which results in a pressure gradient between the two surfaces, which in turn, generates a force.

The angle of attack, the shape and size of the foil and the properties of the incoming fluid flow are the main parameters which influence the hydrodynamic forces generated by the fin.

In order to be able to quantify the lift force, the drag force and the pressure distribution on a wing, coefficients can be calculated, these are dimensionless numbers, which are useful to compare between different profiles and wings. The lift, drag and pressure coefficients are most commonly used to compare between wings or profiles, they are defined as follows for 3D wings.

$$C_L = \frac{L}{\frac{1}{2}\rho_\infty V_\infty^2 S} \tag{2.25a}$$

$$C_D = \frac{D}{\frac{1}{2}\rho_\infty V_\infty^2 S} \tag{2.25b}$$

$$C_p = \frac{p - p_\infty}{\frac{1}{2}\rho_\infty V_\infty^2} \tag{2.25c}$$

The graph from figure 2.6 shows the variation of the lift coefficient with the angle of attack for two

different profiles. Here, it can be seen that the lift force has a linear variation with the AoA for small angles until a critical point, where the flow around the foil separates, and the aerofoil enters stall. In stall, the flow separates from the aerofoil, diminishing the pressure difference between the outer and inner surface, which causes the foil to lose the ability to produce lift. At around 20 degrees for the symmetric profile, the critical point is reached and the foil enters stall, which is explained in figure 2.7.

In the symmetrical profile, the lift at 0 degrees is 0, where as in the cambered one, the profile is able to generate lift from a negative angle of attack. The windsurf fin studied is an example of a symmetrical hydrofoil.

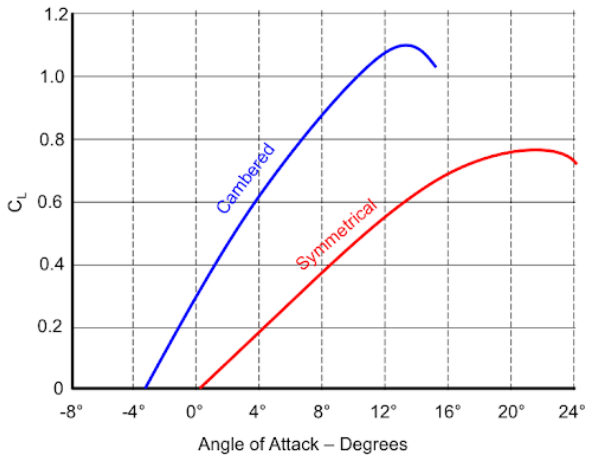

Figure 2.6: Lift Coefficient vs Angle of attack for two foils

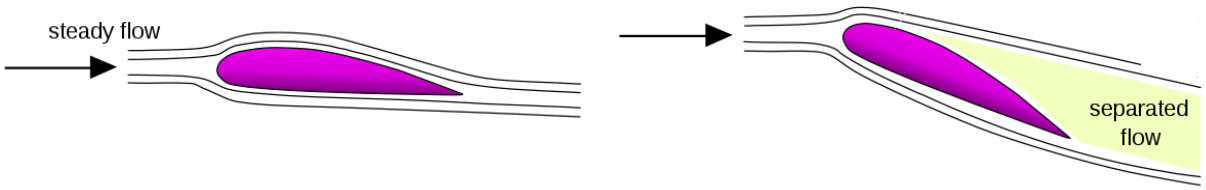

Figure 2.7: Representation of a steady foil (left), and a stalled flow(right

Chapter 3

Structural Model

3.1 Fin Design

In this Thesis a slalom windsurf fin was studied. The fin, presented in figure 3.1, is manufactured by F-Hot, a leading supplier of fins to professional sailors, and has a 37 centimeter length, or span, 10 centimeters root chord, and a rake angle of 2^{o} to the aft. The leading edge of the fin being the round front, while the trailing edge is the straight side.

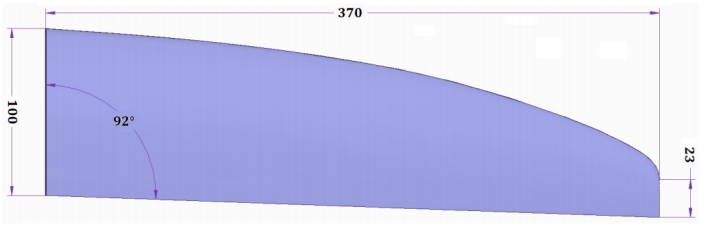

Figure 3.1: 37cm Windsurf Slalom Fin, produced by F-Hot

The profile of the fin can be seen in figure 3.2, it has a maximum relative thickness of 8.10% and it is located at x/c=40%.

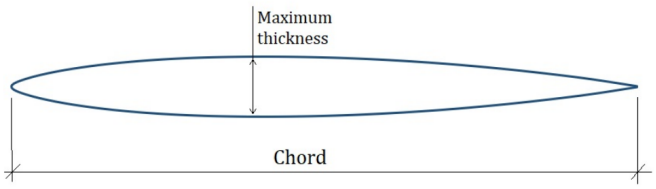

Figure 3.2: F-Hot Windsurf Slalom Fin profile

As for the composite laminate of this fin, each half is composed of 19 layers of carbon and glass fibres in a matrix of epoxy resin. There are 3 different fabrics that compose this laminate: carbon woven, carbon UD and E-glass UD. The layup scheme for the laminating process is as follows:

- 3 layers of carbon woven fabric at an angle of 45° in relation to the trailing edge

- 11 layers of carbon UD fabric at 0° with the trailing edge
- 5 layers of E-glass UD fabric at 0° with the trailing edge

3.2 Software

The first step of the process towards developing this tool was to build a Finite Element Analysis model. There have been other FEA models built previously in this line of work however none had been previously developed in the software needed, ABAQUS, so the FEA model was built from scratch. ABAQUS 2018 was the software chosen due to, in particular, its performance at modelling composite materials and, of course, the availability to connect with a CFD software, Star-CCM+.

3.3 FEA Process

The FEA is a 3D analysis of the windsurf fin, which intends to learn more about the behaviour of the fin. The development of an FEA model is an iterative process, with each step having the need to be validated before moving to the next one. The overal FEA process has multiple steps, which are exemplified in figure 3.3. For more details about the solvers used in the simulation, a book by Barbero can be consulted. [30]

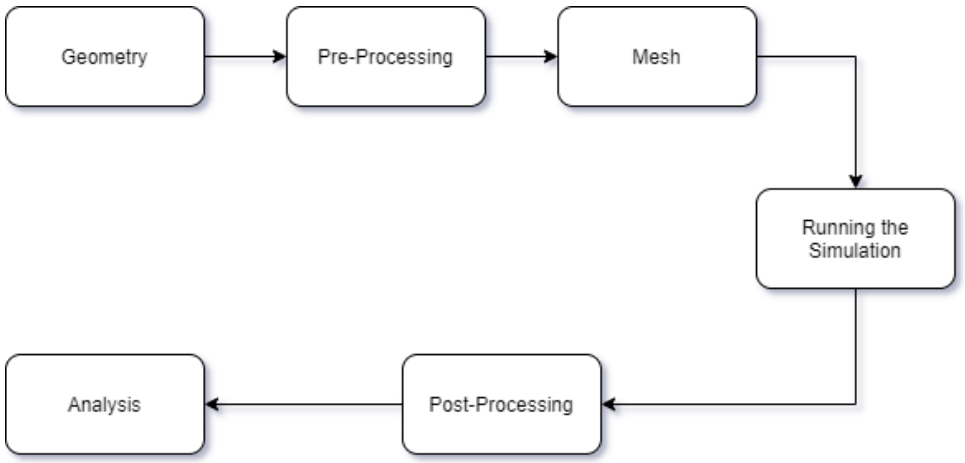

Figure 3.3: Diagram of a FEA analysis

3.3.1 Geometry

The first step towards developing a new FEA model is to have a sound basis, which in this case means to have the best geometry possible to represent the slalom fin which we want to analyse. The initial Computer-Aided Design (CAD) model was developed using the points from a Computer Numerical Control machine used to produce the fin moulds. Afterwards, the available physical model was measured with calipers at various sections throughout its span, the length of the fin, and compared with the available CAD model. Discrepancies were found in this measurements, therefore changes were made to the

geometric model (old file), so that the new model, which will be used in the FEA model (new file) is as close as possible to the experimental one.

The lack of symmetry in the CAD model, failure of closing of the trailing edge (TE) and wrong chord and span dimensions, were some of the problems solved with the development of the new geometry.

Table 3.1: Fin Dimensions

Span [mm]	0.25 chord thickness [mm]		
	Measured	Old File	New File
0	7.51	7.36	7.46
44	7.51	6.88	7.37
88	7.30	6.32	7.17
132	7.05	5.6	6.90
148	6.90	5.39	6.78
176	6.65	4.96	6.54
220	5.97	4.3	6.04
264	5.36	3.57	5.36
296	4.72	3.11	4.69
308	4.34	2.9	4.39
352	3.11	2.17	3.18

As can be seen from table 3.1, the new geometry file is much more accurate in terms of chord thickness compared with the real geometry being studied, which will lead to better results due to a more refined surface for the fluid and a more accurate deflection in the FEA.

3.3.2 Pre-Processing

The second step in the development of a FEA model is to obtain the material properties that most accurately represent the reality, while agreeing with the theory mentioned in section 2.2. In this section, the final material properties used in the simulations are presented. The first and most influential property is the FVF. Taking into account information from multiple papers, by Smith [35] and Sleight [36], and doing an iterative process during validation explained in section 3.4, the FVF chosen were:

$$FVF = 0.35 \text{ for Woven Roving} \tag{3.1}$$

$$FVF = 0.4 \text{ for unidirectional carbon and glass} \tag{3.2}$$

Knowing the density of each material from library values [24]:

$$\rho_{matrix} = 1140\ kg/m^3 \tag{3.3a}$$

$$\rho_{carbon} = 1800\ kg/m^3 \tag{3.3b}$$

$$\rho_{glass} = 2600\ kg/m^3 \tag{3.3c}$$

The density of each composite can be easily obtained by multiplying the density of each material by its FVF, from equations 2.2, resulting in:

$$\rho_{E-glassUD} = 2600 * 0.4 + 1140 * 0.6 = 1724\ kg/m^3 \tag{3.4}$$

$$\rho_{CarbonUD} = 1800 * 0.4 + 1140 * 0.6 = 1404\ kg/m^3 \tag{3.5}$$

$$\rho_{CarbonWR} = 1800 * 0.35 + 1140 * 0.65 = 1371\ kg/m^3 \tag{3.6}$$

Next, there is a need to define the elastic modulus, Poisson's Ratio and shear modulus to use in our model. Starting with the initial values from the ANSYS library, defined in table 3.2 [24].

Table 3.2: Ansys Material Properties of Composites

Parameter	Epoxy E-glass	Epoxy Carbon UD	Epoxy Carbon WR	Units
E_x	3.5E10	1.23E11	5.92E10	Pa
E_y	9E9	7.78E9	5.92E10	Pa
E_z	9E9	7.78E9	7.50E10	Pa
ν_{xy}	0.28	0.27	0.04	-
ν_{yz}	0.4	0.42	0.3	-
ν_{xz}	0.28	0.27	0.3	-
G_x	4.7E9	5E9	3.30E9	Pa
G_y	3.5E9	3.08E9	2.7E9	Pa
G_z	4.7E9	5E9	2.7E9	Pa

And the material properties for the different types of fibres, mentioned in table 3.3.

Table 3.3: Fibre and Matrix Properties [24]

Parameter	Epoxy E-glass	Epoxy Carbon UD	Epoxy Carbon WR	Units
E_{fL}	7.3E10	2.30E11	2.30E11	Pa
E_{fT}	7.3E10	2.30E11	2.30E11	Pa
E_m	3.30E9	3.30E9	3.30E9	Pa
ν_{fLT}	0.22	0.2	0.2	-
ν_{fT}	0.22	0.4	0.4	-
ν_m	0.35	0.35	0.35	-
G_{fLT}	2.99E10	9E9	9E9 6	Pa
G_{fT}	2.99E9	8.21E9	8.21E9	Pa
G_m	1.22E9	1.22E9	1.22E9	Pa

Having all these material properties, the process that was explained in section 2.2 is followed to arrive at the final material properties used in the simulation model.

Firstly, the thickness of each ply is calculated using equation (2.4). For the computational model, the values of the fibre area weight used are 100, 200 and 250, for UD carbon and the first layer of WR, rest of the layers of WR and glass, respectively. Along with the densities mentioned above in equation (3.3), all the necessary data is known to calculate the thickness of each layer. Final thicknesses are presented in table 3.4.

Table 3.4: Thickness of the computed composite layers

Woven Roving 100	Woven Roving 200	Unidirectional Carbon	Unidirectional glass
0.1623 mm	0.3247 mm	0.1374 mm	0.2451 mm

Using the equations from section 2.2, where all the theoretical reasoning behind each assumption made was explained, the remaining material properties calculation is straightforward. With the final composite material properties results being summarized in table 3.5.

Table 3.5: Final Composite Properties

Parameter	Epoxy E-glass	Epoxy Carbon UD	Epoxy Carbon WR	Units
E_x	2.23E10	5.66E10	2.84E10	Pa
E_y	7.9E9	5.11E9	2.84E10	Pa
E_z	7.9E9	5.11E9	5.54E9	Pa
ν_{xy}	0.29	0.31	0.04	-
ν_{yz}	0.4	0.42	0.3	-
ν_{xz}	0.29	0.31	0.3	-
G_{xy}	4.12E9	3.26E9	3.3E9	Pa
G_{yz}	3.50E9	3.08E9	2.70E9	Pa
G_{xz}	4.12E9	3.26E9	2.70E9	Pa

After having all the material properties properly defined, the next step of the FEA process is to build the model. This step depends on the software being used, however, in ABAQUS, there is a need to partition the geometry in different “pieces” so the software can properly mesh the geometry. In this model, the partitions, that can be seen in figure 3.4, also help to define the position of each ply in the fin. The model is composed by 38 plies of different widths (50 and 70 mm) many different lengths (from 14 cm to 24 cm) and different composite materials, along with a “skin” layer, for the resin used on the mould, and an “epoxy” layer, which defines the paste used to fill the vacant spots between each side of the fin.

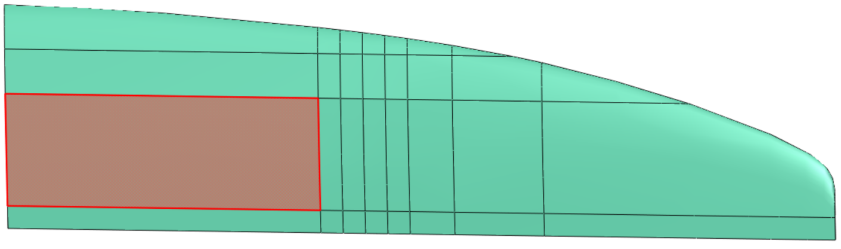

Figure 3.4: Partitions made in ABAQUS

In this case, the partitions in the horizontal direction limit the width of the plies to 50 mm and 70 mm, and the vertical partitions limit the length of each ply. Only one partition in the thickness direction was made, through the middle of the fin, to ensure symmetry relative to this plane. This set of partitions is enough to fully characterize the plies, because the thickness of each composite is an input of the program, which removes the need to have more partitions in the thickness direction. This was critical, because otherwise the FEA file would be too large to be easily changeable, something which is of the utmost importance when doing a parameter study and to have a final tool which is easy to use.

The choice of element is also a critical decision in the FEA process, in this case, taking into account what was said in sections 2.3.1, 2.3.3 and 2.3.2 the continuum shell element was chosen. The continuum shell element was chosen due to the inability of the conventional shell elements of defining the inner epoxy layer, since it does not have a pre-determined shape, it simply fills up the fin. In addition to this, it is the more precise element when compared to solid elements, due to the complex shape of the fin.

There are two methods of implementing a composite set in ABAQUS, through the inputs in ABAQUS CAE, use a composite layup or simply define a composite set. The decision of using a composite set was made because a composite layup must be associated to a single element through the thickness of a region [30], this would cause problems due to the composite layup being replicated in each mesh cell and decrease the quality of the mesh if it was to be implemented.

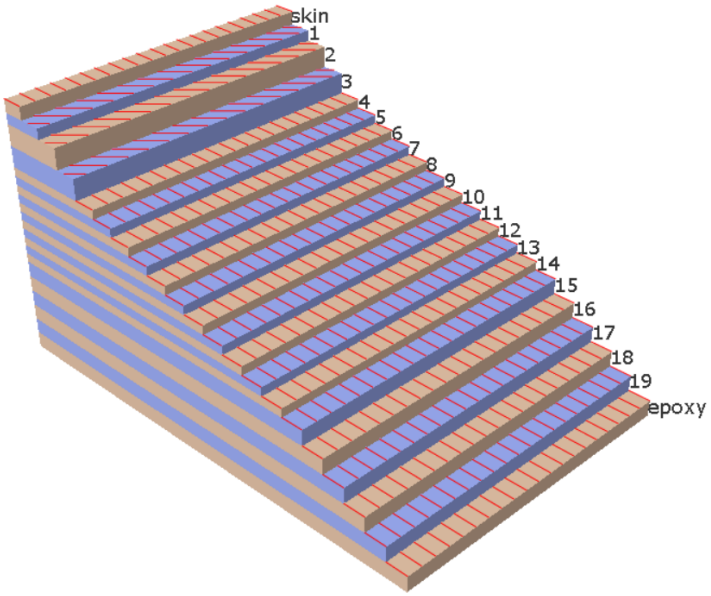

Figure 3.5: Ply orientation in ABAQUS

Having defined through the partitions all the sections needed to properly emulate the windsurf fin, each section will be ”filled” with the corresponding plies. In figure 3.5, it is observable the distribution of plies and its orientation for the section highlighted in red in figure 3.4. The distribution and orientation of the plies was defined by taking into account data from the manufacturer. This portion of the fin is filled with all the possible plies due to the fin being manufactured with all plies starting from the top, which means that they forcefully have to go through this section.

At this point in the process, the computational model is ready to be loaded with the boundary conditions and any loads necessary for the study. Figure 3.6, presents the boundary condition at the top of the fin which represents the fin being attached to a windsurf board, restricting both translation and rotation. As well as a concentrated load, applied at 40% span, used in the validation process.

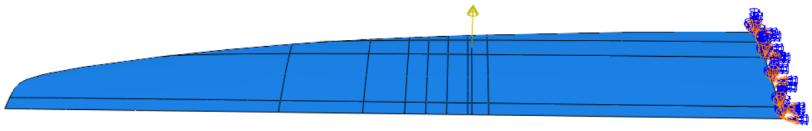

Figure 3.6: Computational model with boundary conditions and external load

3.3.3 Mesh

The final step in developing the FEA model is to mesh the geometry. Due to the choice of continuum shell composite element, the mesh is forced to be a hex composed mesh. As mentioned previously, the partitions that were made to the geometry are essential to the meshing process, without those partitions the geometry is too complex for the ABAQUS software to automatically mesh, since the meshing algorithm struggles with complex geometries, like the windsurf fin.

When meshing in ABAQUS, two effects have to be taken into account: hourglassing and shear locking. Hourglassing occurs in first-order reduced-integration elements, due to these only having one integration point, making it possible for them to distort in such a way that the strains calculated at the integration point are all zero, which leads to uncontrolled distortion of the mesh [31]. In order to prevent this, the mesh should be reasonably fine. Shear or volumetric locking occurs in first-order, fully integrated elements that are subjected to bending. The numerical formulation of the elements gives rise to shear strains that do not really exist, also called parasitic shear.

In this meshing process, the element type chosen was SC8R, a first-order reduced-integration element. Since these types of elements may suffer from hourglassing effects, the generated mesh has to be reasonably fine.

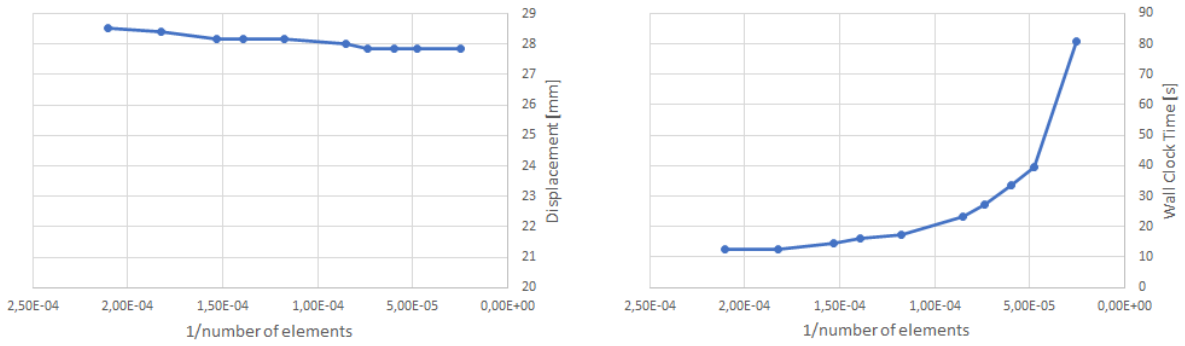

(a) Displacement behaviour with mesh density

(b) Wall-clock time with mesh density

Figure 3.7: Mesh convergence study

A mesh validation study was conducted in order to choose the global size for the FEA mesh. Figure 3.7 shows the convergence study done on the mesh for the 80% span point load case. The mesh size influence was studied both on the displacement of the fin's tip and on the computational cost, represented by the wall-clock time. Taking into account both parameters, the approximate global size of 4 was chosen, which means that the average cell will have 4 mm as its defining size, this results in a mesh with 13824 elements and 7.23×10^{-5} 1/number of elements. This value was chosen for the global seed due to its accuracy on the displacement of the fin, having a relative difference to the finest mesh studied of under 0.1 %. While not having an excessive computational cost, taking approximately a third of the time of the finest mesh.

The final mesh is represented in figure 3.8. As can be seen in figure 3.8, both leading and trailing edges of the fin have zones of refinement, in order to maintain the quality of the mesh as it approaches the edge of the fin. This zone of refinement possesses a lower defining size compared with the overall mesh, and one which diminishes as the mesh approaches the corner of the fin.

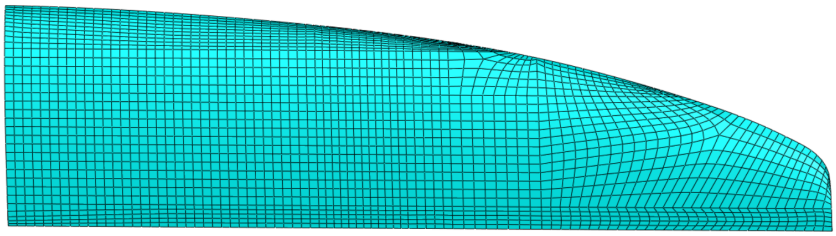

Figure 3.8: FEA mesh on ABAQUS

3.3.4 Post-Processing

After running the simulations several results can be evaluated, such as the deformation of the fin, the maximum stress and more importantly, its location. Another output of interest is the max in-plane stresses in each ply, these outputs help validate the fact that the plies are well-defined in the model and well located in the fin. It is also possible to define the twist of the tip of the fin, having the displacements in all three directions of each mesh node. These displacements along with simple trigonometry can be used to calculate the twisting behaviour for each loading condition. Figure 3.9 shows some results obtained from the FEA software. On the left, the in-plane stress of a single ply can be seen, the stress distribution in this ply confirms what was expected, which is that the area of higher stress is near the top of the fin, where it was built-in the windsurf board. On the right the difference between the model before the pressure load being applied and after, shows that the model is behaving as expected, going away from the root of the fin the displacement increases, being maximum at the tip of the fin. ABAQUS post-processing tool can also be used to verify the ply orientation and confirm the fact that the fibre orientation definition in the model is correct.

3.4 Model Validation

In order to guarantee that all the previous made choices were correct, although they were based in theoretical evidence, a validation process is done. The validation process intends to prove that the modelled fin behaves similarly to the real fin when exposed to the same conditions, such that the results of future simulations will be valid and of interest. This process was used to iterate throughout the development of the FEA model, in order to have the most accurate numerical model possible.

As the composite laminating process is a manual labour, the construction process is not extremely precise, so, when creating the numerical model, there is some margin for changing the physical properties and lay-up of the plies, in order for the numerical results to match experimental ones.

This calibration process was conducted by Nascimento [17] in his thesis focused on the same windsurf fin. The mechanical tests consisted of a point load applied at the hydrodynamic centre of pressure, quarter chord from the leading edge, at 40% and 80% of the fin span which is where the centre of pressure of a semi-elliptic loading generally is, as represented in figure 3.10 .

When experimentally testing the fin, the hydraulic cylinder controlled by a computer and installed perpendicular to the fin's surface, causes a displacement to the Fin at a rate of 0.1 mm/s to simulate a static loading. When deflecting the fin, the probe is systematically calculating the force being exerted

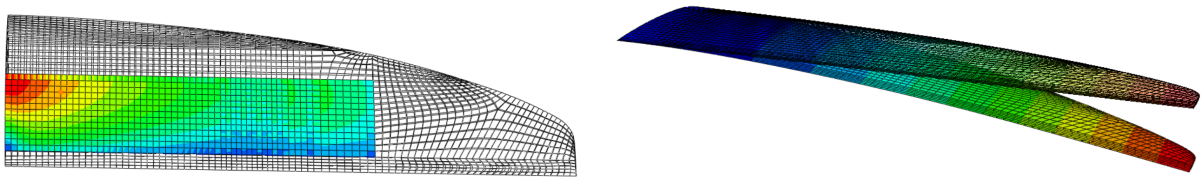

(a) In-plane stress for a specific ply

(b) Displacement

Figure 3.9: Different output options in ABAQUS post-processing

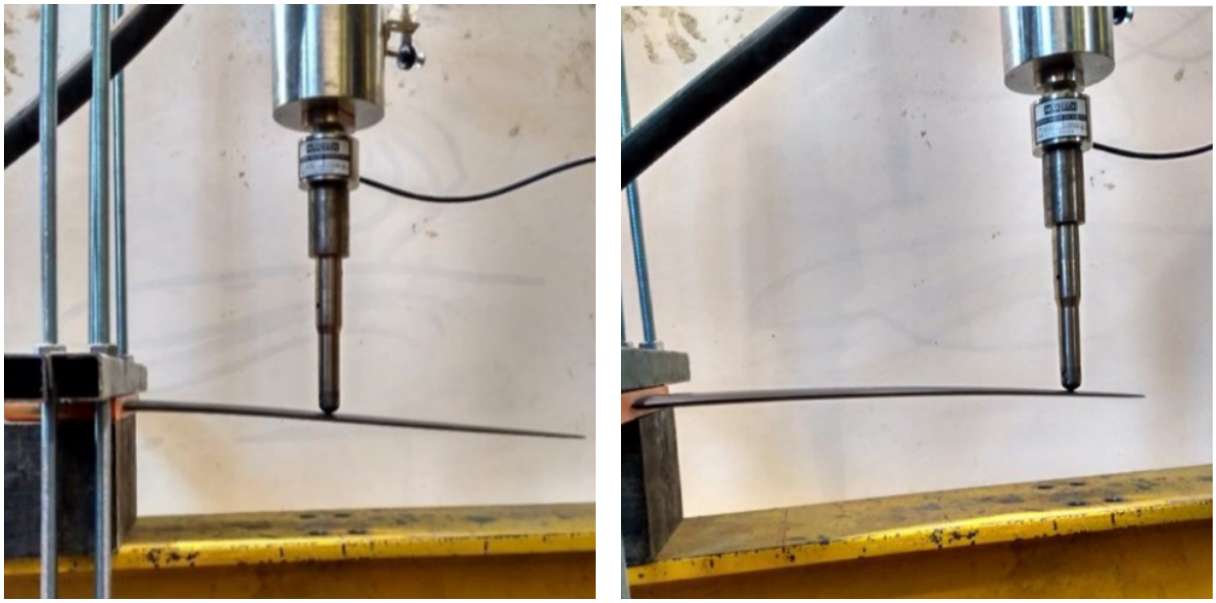

(a) 40% of span

(b) 80% of span

Figure 3.10: Experimental test for point loading analysis: 40% span (left) and 80% span (right)

and the respective deflection caused, in order to then be able to plot the force-displacement behaviour of the fin (figure 3.11). The fin behaves in a linear manner, which means that it is only operating in the elastic domain, which verifies the composite material theory presented in section 2.1.

After running the first numerical models and collecting the results of both tests at 40% and 80% span, a comparison with the experimental data is done. The takeaway from this comparison is that the model is behaving similarly, however the results have a different slope for the force-displacement performance. After many iterations of the calibration process, from changing FVFs, Elastic modules, to ply thicknesses, the final material properties (table 3.5) were decided which produced the results found in figure 3.11, and reproduce closely, with an error of approximately 7% the real life fin behaviour. In this test, the 80% span result is more important, because that point is closer to the hydrodynamic point where the forces will be applied in the windsurf case, and therefore in the FSI process.

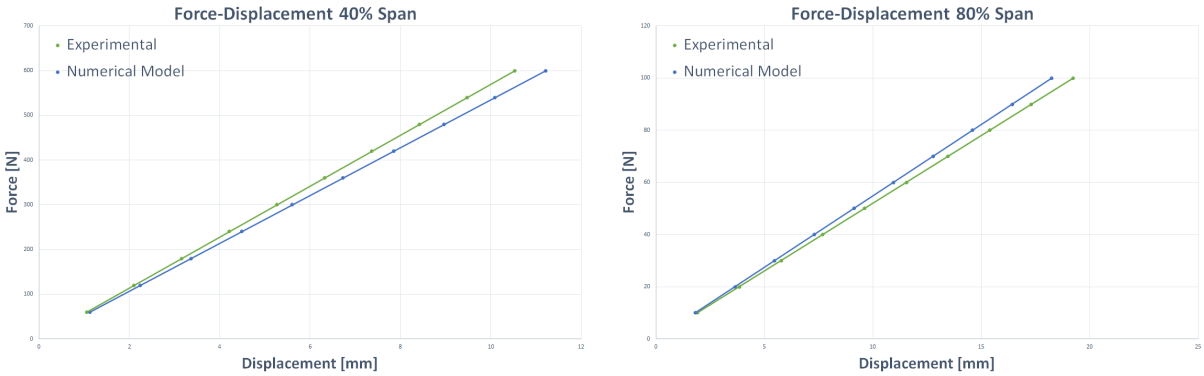

(a) Force-Displacement for 40%span

(b) Force-Displacement for 80%span

Figure 3.11: Force-Displacement graphics for both 40 (left) and 80 (right) % span cases

In this chapter, the development of the structural model was discussed and the major steps in the creation of this model were explained and analysed. Particularly, the set-up of the material properties and plies inside the fin, as well as the generation of the mesh. Some of the post-processing tools of ABAQUS were also mentioned. After having developed the structural model, the next step in the path to the final design tool is to build a hydrodynamic model.

Overall, 5 computational hours were spent running the FEA simulations.

Chapter 4

Hydrodynamic Model

The second step in the process of developing this analysis tool was to build a CFD model in Star-CCM+. The CFD analysis of the fin computes the pressure distribution around the fin, induced by the movement of the fluid, which will then be imported into the FEA model to study how the fin behaves when hydrodynamically loaded.

4.1 Sailing Conditions

The fluid flow used in the simulations completed during the process of this work is seawater with a salinity of 35 g/kg [37].

The study of the slalom windsurf fin was tested for some specific conditions, which are presented in table 4.1.

Table 4.1: Operating Conditions for the simulations on the windsurf fin

Parameter	Value	Units
Temperature (T)	20	°C
Density (ρ)	1024.9	kg/m^3
Dynamic Viscosity (μ)	1.077E-3	$Pa \cdot s$

Table 4.2: Input parameters for the simulations on the windsurf fin

Parameter	Value	Units
Angle of attack (AoA)	2, 4, 6	degrees [º]
Speed	10, 15, 20, 25, 30, 35	knots

The input parameters used in this study are the ones presented in table 4.2. The reason for the chosen angles of attack is that the values fall into the range of angles of attack where flow separation, or stall, does not occur and are frequent drift angles when windsurfing. There were two reasons behind the choice of speeds, the standard speeds at a slalom windsurf event and pushing the limits of the fin design and construction, with the 35 knots.

Additional conditions for which the fin is numerically tested are related to the fluid continua. The fluid is assumed to have a constant density, to be incompressible, to be steady and turbulent flow. All these conditions are then implemented into the CFD software for the numerical simulations.

4.2 Software

The software used for the computational fluid dynamics analysis was Star-CCM+ 13.06. Star-CCM+ is a very complete numerical simulation software focused on Computational Fluid Dynamics, able to study not only cases involving fluid flow but also heat transfer and structural stresses [38]. It is an intuitive and easy to use program, and it comprises a CAD modeler, a robust meshing generator, several models and parameters that can be tuned for the purpose of the analysis. It also has very intuitive post-processing analysis features which are very powerful.

The decision to use Star-CCM+ came because of its availability and support at Laboratory and Simulation in Energy and Fluids (LASEF) in Instituto Superior Técnico (IST), especially from Prof. Chaves, my supervisor. It also has powerful simulation competences and it is already known for its good performance when analysing turbulent fluid flow around wing-shaped geometries. Star-CCM+ is also the best CFD software to pair with ABAQUS for a precise and automated FSI analysis.

4.3 CFD Process

The windsurf fin CFD study to be conducted, is a 3D analysis of the referred component. A CFD analysis follows a standard procedure that can be broken down into multiple phases, which you can see in the diagram in figure 4.1. Following, a brief explanation of each phase and of the choice of parameters to use in the simulation.

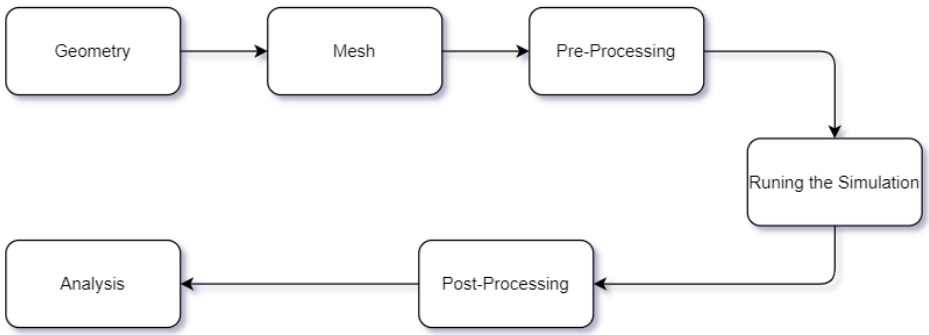

Figure 4.1: Diagram of a CFD analysis

4.3.1 Geometry

The first step, when starting a CFD analysis, is to create the CAD model. Although Star-CCM+ has an integrated CAD designing software, in this project the CAD model was designed in Rhino by Dr.

Sutherland and then altered in SolidWorks by the author. The geometry used in the structural model needed to be altered to be used in the CFD model, due to having a sharp leading edge. Although this is the most simple representation of the fin, it is not totally accurate and it is a problem for the study of the flow around it. Therefore a fillet on the leading edge tip was made, in order to eliminate any singularities and the domain to be studied was also added to the geometry in the same software. This geometry marks an improvement over previous Theses, as was explained in section 3.3.1.

The fluid domain is a rectangular prismatic volume centered around the fin, represented in figure 4.2, which consists of a length of 16 chords, 6 before the fin and 10 after, width of 10 chords and height of 8 chords. The domain extension had been previously validated in previous work [20].

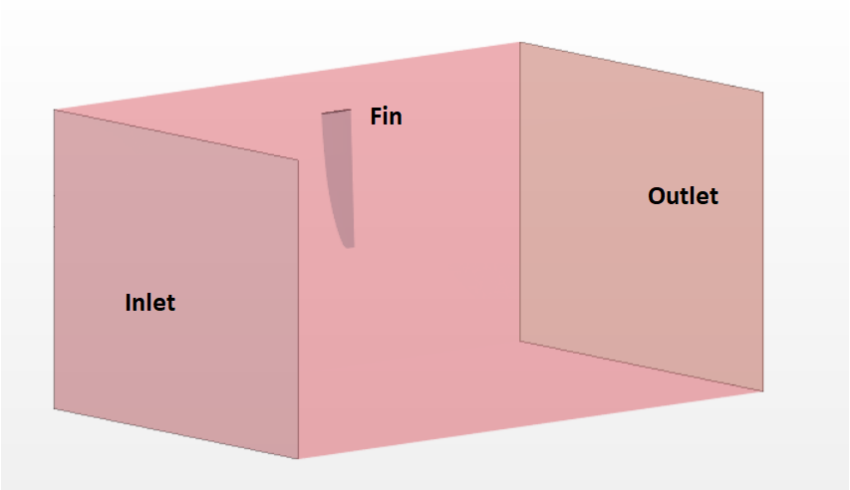

Figure 4.2: Computational Fluid Domain and Boundary Surfaces

4.3.2 Mesh

The second major step in developing a CFD model is the mesh generation. In order to generate a mesh, every surface has to be identified, assigned to a specific region and be identified with a type of boundary condition. In this analysis, the boundary conditions used are: *Velocity Inlet* for the Inlet and side surfaces, *Pressure Outlet* for the outlet surface, and *Wall* for the Fin surface.

The mesh is then created using the *Automated Mesh* feature of Star-CCM+, with the characteristics of the grid chosen based on previous research [20]. The used meshers were : *Surface Remesher, Polyhedral Mesher,* and a *Prism Layer Mesher*.

The mesh is not uniform across all the domain because, to have the accuracy needed in the areas of interest, close to the fin, there would be a need for a very large number of cells. In order to save computational space and, at the same time, accurately determine the responses of the fin to the surrounding fluid, Volumes of Refinement (VOR) were created. The most important VOR is the one closest to the fin, which in this study was constructed to have an approximate geometry of the fin being studied, albeit slightly larger so it envolves it. The shape used for the VOR is very impactful on the computational cost, as a VOR that closely hugs the shape of the fin allows for more precise analysis when compared with a simple block. These VOR improve the performance of the prism layer meshing, which is useful to

analyse the boundary layer, and the performance of the overall mesh due to a more accurate definition of the fluid around the fin. This marks a significant improvement over previous work done on this topic.

The mesh used in all CFD and FSI simulations, presented in figure 4.3, has the following main characteristics, presented in table 4.3.

Table 4.3: Mesh main parameters

Base size	0.05 m
Number of Prism Layers	25
Prism Layer Thickness	0.002 m
Prism Layer Stretching	1.17
Wall y+	approx. 1
Domain Relative Cell Size	150%
VOR 1 Relative Cell Size	3%
VOR 2 Relative Cell Size	10%
VOR 3 Relative Cell Size	50%
Number of Cells	3M

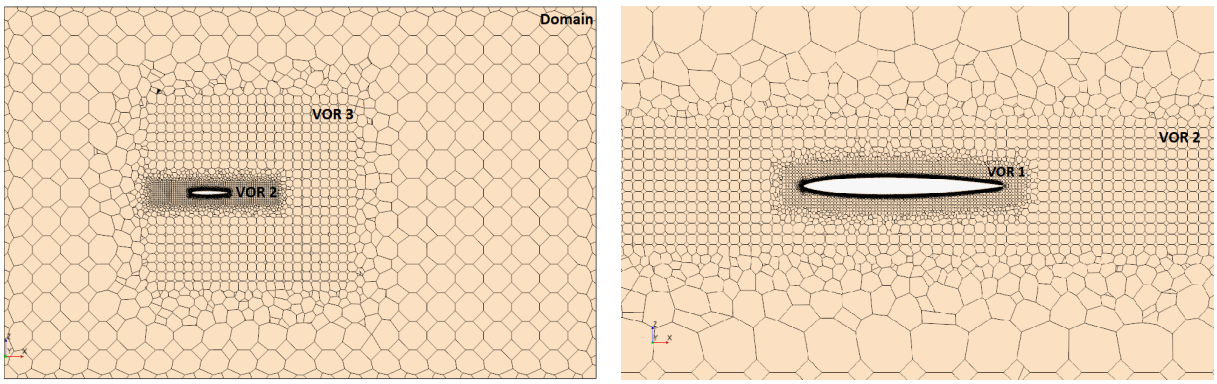

(a) Overall CFD mesh

(b) Mesh around the fin

Figure 4.3: CFD mesh on Star-CCM+

4.3.3 Pre-Processing

Another very important step in developing a CFD simulation is the pre-processing, this includes setting up everything for the simulation to run, from physics continuum properties to initial values for pressure, density and velocity in all boundary conditions.

The following physics continuum models were used for all CFD simulations, all of these model have been studied extensively, therefore no in-depth analysis will be made. The choice of physical models such as the turbulence model had been made in previous work [20].

- Three-Dimensional Analysis
- Steady and Segregated Flow
- Constant Density

- Turbulent Flow solving the Reynolds-Average Navier-Stokes equations
- K-ω, SST (Menter) Turbulence Model
- $\gamma - Re_\theta$ Transition Model
- Low y+ Wall Treatment

4.3.4 Running the Simulation

The next step in the CFD process is running the simulation, until solution convergence occurs. The convergence of the numerical results is a fundamental part of the simulation process, as it does not present meaningful results if the residuals do not converge. The criteria used to know if the simulation has converged is usually the residual values and the analysis of a specific quantity of interest.

Residual values are one of the most fundamental measures of an iterative process convergence, as it quantifies the error in the solution of the governing system of equations. In an iterative numerical solution, the residual will never be exactly zero. However, the lower the residual value is, the more numerically accurate the solution for a given mesh. For CFD purposes, residual values inferior to 10^{-4} are the threshold for a loosely converged solution.

Another way to check for convergence is to analyse the evolution of a specific quantity over multiple iterations. In a steady state analysis, for a converged solution, the numerical results between two iterations should be negligible. So, it is possible to monitor the evolution of a specific parameter and check if there is a negligible variation between consecutive iterations.

For the specific study of the windsurf fin, the convergence criterion used was the convergence of the residuals. However, as you can see in the figure below 4.4 a negligible residual value translates to a constant lift value.

In some cases, the solution did not satisfy the convergence criteria, usually due to the residuals of the turbulent kinetic energy, which is predictable due to some very quick phenomenons. An analysis was made to investigate the influence of these events on the final solution. In this case, this will not affect the results since they occurred away from the fin.

In the search for convergence of the residual values, some parameters of the simulation can be tuned. A small refinement of the mesh can be done, specifically near the fin's surface. Relaxation Factors (RF) can be changed, particularly changing the velocity RF to 0.5, the pressure RF to 0.1 and the turbulence RF to 0.5. Finally, changing the analysis from a steady solution to an unsteady one, especially one with a very small time-step, can get rid of very quick phenomena which would otherwise impact the residuals convergence.

The Relaxation Factor is a coefficient often used in iterative solvers, when solving iterative non-linear equation systems a solution may start to diverge. In theses cases, a under-relaxation factor (RF$<$1) is used to help the solution stabilize and to get to converged results. This translates to using a combination of the previous step results with the new step results, instead of only using the new step results to make sure that there is no significant changes. An over-relaxation factor (RF$>$1) can also be used in iterative

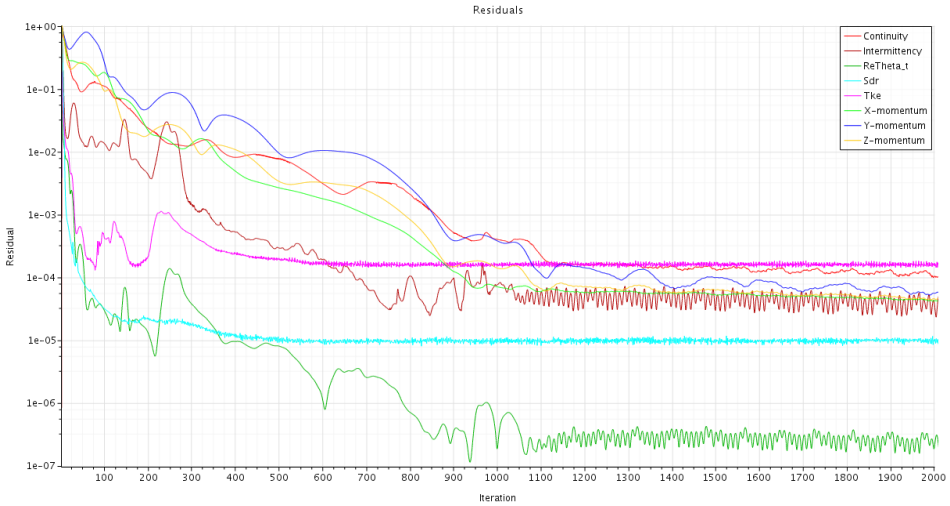

(a) Residuals graph

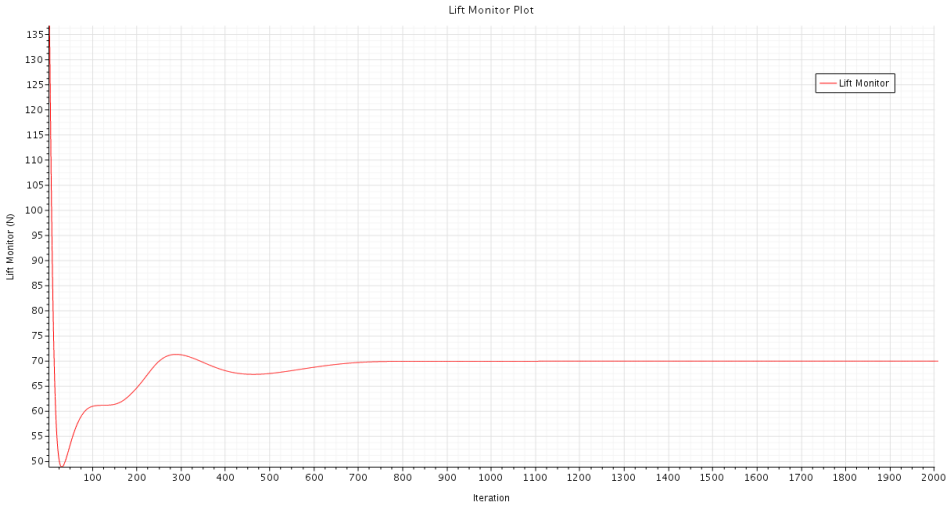

(b) Lift Force graph

Figure 4.4: Graphics for the case of 10 knots and 2º AoA

processes, this is often used when the user is confident that the solution is on its way to convergence as a way to speed up the process. In these cases, the next step solution will be multiplied by a factor, increasing its “importance”.

Each simulation took 180 computational hours, running in 18 cores simultaneously.

4.3.5 Post-Processing

Finally, to be able to take conclusions about the finished simulations, a post-processing analysis is done. Star-CCM+ has very powerful and simple post-processing features, with the option of generating multiple plots, scenes and reports. In the case of the present work, the post-processing analysis consists of visualizing streamlines and other color mapped data that capture laminar separation bubbles and pressure distribution, as well as plotting the lift and drag forces evolution. The pressure and velocity field are very important for the user to know if the simulation is behaving as expected, as well as generating

scenes with high residual locations, which give more information about where and why any potential errors are occurring. In figure 4.5 a), it can be seen the wall y+ parameter represented on the fin's surface, which is expected to be around 1, this scene gives information to the user regarding the accuracy of the prism layer. If the wall y+ parameter is too low, the prism layers are often too small, not allowing the information to flow through. In figure 4.5 b), the flow around the fin is represented through a vector field, this type of scene gives information about the boundary layer, the existence of any separation bubbles and the overall behaviour of the flow around the fin.

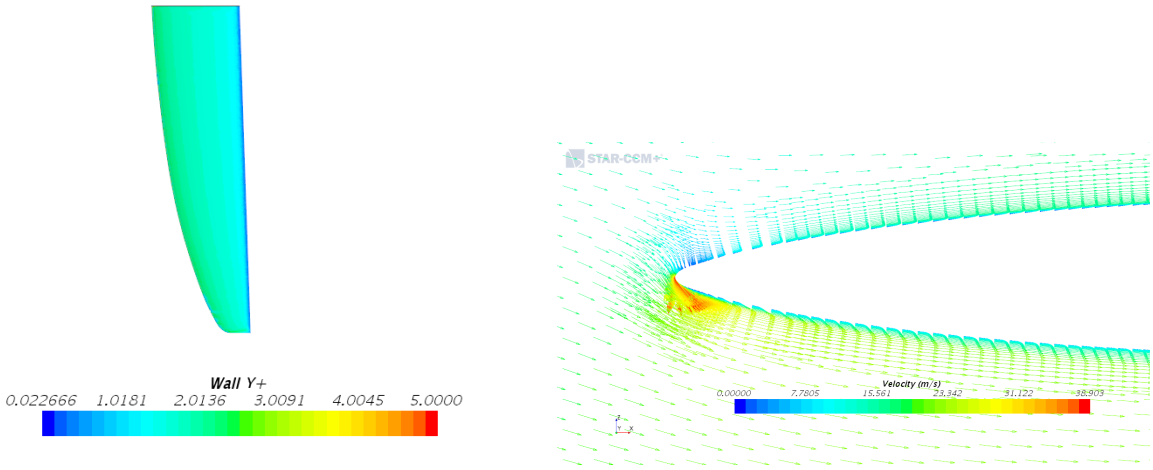

(a) Wall y+ parameter on the fin's surface

(b) Velocity field vector around the fin's leading edge

Figure 4.5: Post-processing scenes in Star-CCM+

A combination of knowledge in the CFD process, as well as, knowledge of fluid mechanics is very important when analysing computational simulations. One can not take for granted the values that the computer gives, instead making a reasonable and thoughtful analysis of the results.

In this chapter, the process of developing a CFD model in Star-CCM+ was described, in particular the choice of meshing parameters and physics continuum properties, which had been previously selected. The convergence criteria for a CFD simulation was established and some of the post-processing features of Star-CCM+ were explored. At this point, both the structural and hydrodynamic model are fully developed and ready to be coupled in a FSI analysis.

Chapter 5

Fluid-Structure Interaction Model

The Fluid-Structure Interaction (FSI) is a process that studies the interaction between a deformable structure and its surrounding fluid, through a coupling of the laws that describe each scenario. In most flow problems, there are two domains, a fluid and a solid one, however this does not imply that there is a need to perform an FSI analysis. This analysis is only relevant when the interaction is found to be significant [39].

This coupled analysis is of extreme importance in multiple engineering fields, being very important to properly define the behaviour of a solid structure immersed in moving fluid flow, such is the case of wind farms for renewable energy or the case of airplanes due to oscillatory phenomena that can lead to flutter.

In a typical single-field mechanics problems, be it a fluid-only or a structure-only problem, the simulation starts with a set of governing equations in the domain and a set of boundary conditions on the domain boundary [40]. It is much more complicated in a FSI problem such as the one being studied here, because both sets of differential equations and boundary conditions must be satisfied simultaneously.

The two domains are interconnected through a common physical interface surface, through which information about both analysis is transmitted. The interface condition is the compatibility of the kinematics at the fluid-structure interface. The two main concepts that need to be understood in order to set up a FSI analysis correctly, are the time discretization and the morphing of the mesh.

5.1 Time discretization

There are two main methods for the coupling of the fluid and structural simulations, one-way and two-way coupling .

One-way coupling is used in problems where the fluid forces have a small impact on the structure shape, the structure is rigid enough so that the flow is only affected marginally. This method has a very efficient computational time, however it does not guarantee energy conservation at the interface, affecting the stability of the results.

Two-way coupling methods are further divided between explicit and implicit coupling algorithms, also

known as weak and strong coupling respectively. In two-way interactions the fluid motion and pressure affect the displacement and deformation in the structure, and the response of the structure has a significant effect on the flow field [38].

In the weak coupling method, or explicit coupling, the convergence at the boundary between the structure and the fluid is not considered, and a new step is launched directly. This approach often leads to more efficient computational time than the strong approach, with the drawback that the inertia effects are neglected and the two solvers are not achieving convergence at the same point in time.This method should be used in applications where the effect of the structure on the fluid is much larger than the effect of the fluid on the structure [38].

In strong, or implicit, coupling a converged solution for the flow field is required to provide the forces acting on the body at every time-step. After interpolating the forces from the fluid mesh to the surface mesh of the structure, a converged solution of the structural dynamics needs to be achieved under the effects of the acting forces. The response of the structure to the load represents a displacement of the structural nodes. The displacements at the boundary between the structure and the fluid are interpolated to the fluid mesh, through a mapping process, which leads to the deformation of the mesh through morphing. This process closes one inner loop of the simulation. All these steps are repeated until the changes in displacements and flow forces fall below a prescribed threshold. Afterwards a new time-step is started [41].

5.2 Mesh morphing

The deformation of the fluid grid by moving the fluid vertices to conform to the solid structure in order to maintain a reasonable quality fluid grid is called morphing. This arbitrary motion of the fluid mechanics domain needs to be accounted for in the differential equations and boundary conditions. The technique used to solve this problem is the Arbitrary Lagrangian Eulerian (ALE) technique [42], the key word being arbitrary, as the mesh points movement is random except that it must conform to the moving structural boundary and it must provide a reasonable quality mesh. ALE allows this by taking the convection of these points into account.

In solid mechanics, a Lagrangian formulation is applied, so that a portion of the computational domain represents a portion of the solid body. As a result, motion of the solid mesh corresponds to motion of the solid body. Fluid mechanics applies an Eulerian description, so that a portion of the computational domain represents a portion of space through which material flows [38]. ALE combines the two approaches which allows a control of the mesh geometry independently from the material geometry [43].

On the interface surface the data is mapped from the fluid solver to the structural solver and vice-versa. In the Co-Simulation Engine a shape function interpolation is used to map the fields between a boundary on the fluid grid and a surface on the structural mesh, using a model like in figure 5.1. A separate mapping operation is done for each type of field exchanged.

Further details on the fluid-structure interaction model, the time discretization and other chosen parameters can be found in section 5.4.1.

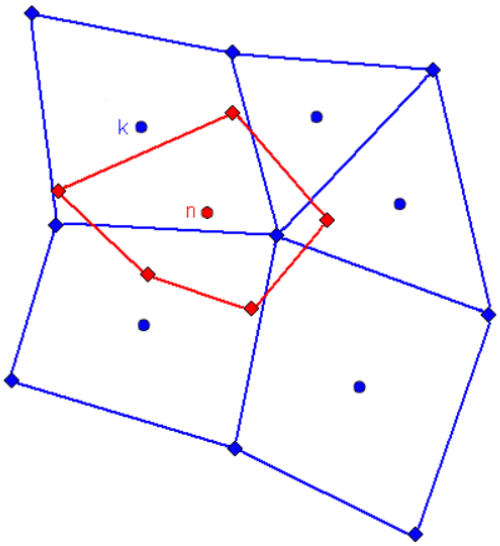

Figure 5.1: Solution Data Interpolation diagram [38]

An automated FSI analysis was proposed for this work due to the need of a design tool that accurately predicts the behaviour of the Windsurfing fin when in operation.

A one-way FSI analysis with a single iteration, where a structural analysis of the Fin was done using a pressure load obtained by extrapolation from the results of a 2D hydrodynamic study, was done in previous studies [18] [19] . A two-way FSI analysis was also done previously, where the author did the iterations manually due to limitations with the computational model [20]. This work is an improvement over previous attempts, because a two-way FSI analysis with automatic iterations will be done. This hydroelasticity analysis will predict the behaviour of the fin with higher accuracy due to less limitations with the number of iterations and less errors with the exchange of data between the two domains.

5.3 Software

Having done both the structural and hydrodynamical models, with ABAQUS 2018 solving the structural domain and Star-ccm+ 13.06 solving the fluid domain, both models are now going to be connected through the Co-Simulia Engine (CSE). CSE allows both softwares to communicate with each other, importing and exporting field properties as well as mesh information. The CSE is a fully automatic way of doing two-way coupling, which for problems such as this one, where both analysis influence each other, is very important.

5.4 FSI process

Similarly to the CFD process mentioned in section 4.3, a FSI analysis will follow a standard procedure, broken down into multiple phases in figure 5.2. The main difference between CFD and FSI analysis being the aspect of communication with another software in between the multiple iterations.

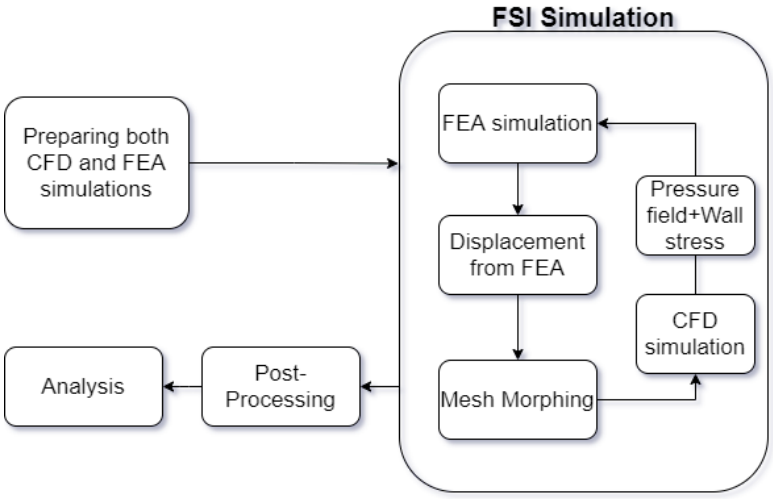

Figure 5.2: Diagram of a FSI analysis

5.4.1 Pre-Processing

The FSI analysis can only be initiated after having developed both FEA and CFD models previously, however these simulations have to be slightly altered in order to be able to communicate with one another while running. It is very important to correctly define the co-simulation controls both in ABAQUS and Star-CCM+.

The same surface must be present and defined with the same name in both solvers. In this region the displacements will be exported from the FEA solver and the pressures normal to the element surfaces, as well as the wall shear stress are imported from Star-CCM+ to ABAQUS [31]. Extra attention has to be given to the simulation's units, due to the fact that ABAQUS does not have an integrated units system. In this case, since the geometry was constructed in millimeters, all units have to be in accordance to this which, in the case of pressure, for instance, is MPa instead of the SI Pa.

The approach chosen to model the FSI coupling between the structure and the fluid is a dynamic implicit solution, as there is a strong physical coupling due to the fact that the composite made fin is lightweight and highly flexible. As mentioned previously, in section 5.1, in the implicit iterative approach, the fields are exchanged multiple times per coupling step until an overall equilibrium is achieved prior to advancing to the next coupling step.

The iterative coupling scheme allows one analysis to lead, highly recommended to be the structural solver, in this case ABAQUS, while the other analysis lags the co-simulation [38]. The structural analysis uses the data from the previous time-step, as the initial prediction of the fluid loads at the end of the current time-step.

Lastly, the coupling step size needs to be specified in both solvers, which will define the period between two consecutive exchanges, in this case 0.1s. This coupling step size was established after many iterations with different time steps were unable to converge, either due to the step-size being too big or too small. Also in this study, it was found that the step size of both softwares should be constant. The coupling step size is established at the beginning of each coupling step and a constant coupling size will be used, allowing both analyses to advance in parallel. In the following equation, δt_c defines the

coupling step size, t_{i+1} is the target time, or the next iteration time, and t_i is the current time at the start of the step

$$t_{i+1} = t_i + \delta t_c \tag{5.1}$$

Finally, a study on the use of a ramping parameter of the pressure was done. It was found that not using a ramping model led to the solution diverging rapidly and the simulation being unable to run, especially for operating conditions where the deflection and expected pressure field on the fin would be higher. The ramping time and the total displacement define the rate at which the fin deflects. Thus, when expecting more deflection, higher ramping time was used. Otherwise, the simulation cannot withstand the large pressure differences that would occur with a smaller ramping time. This is particularly important at the start of the simulation, since the structure is initially unloaded and the initial flow field is calculated with a rigid structure. The initial parameter was set to 0 in the Co-Simulation Time and the second parameter was increased along with the velocity and the angle of attack, due to an expected higher deflection.

5.4.2 FSI simulation

The same criteria used in the CFD simulation, explained in section 4.3.4, were used for the convergence of the FSI simulation. In figure 5.3, it can be seen that the residuals of the simulation are all around the value of 10E-4, which is the goal and in figure 5.4 that the displacement calculated by ABAQUS stays consistent once the residuals start to lower. Confirming the connection between the residual values and the stabilization of a specific quantity of interest, in this case, deflection.

Each simulation took 216 computational hours, running in 18 cores simultaneously.

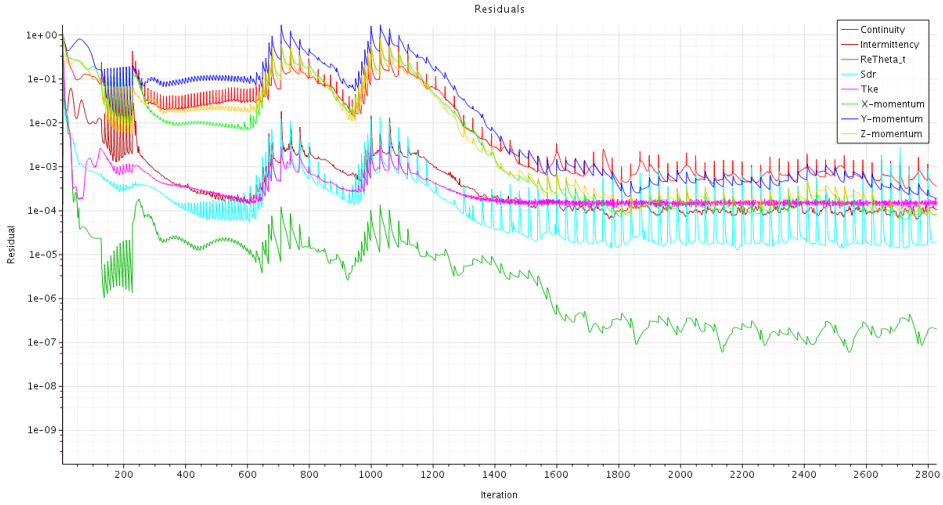

Figure 5.3: Residuals graph from Star-CCM+

5.4.3 Post-processing

Similarly to the CFD process, a post-processing step is of paramount importance to understand and analyse the data collected. Contrary to the previous case, the post-processing here will be made with

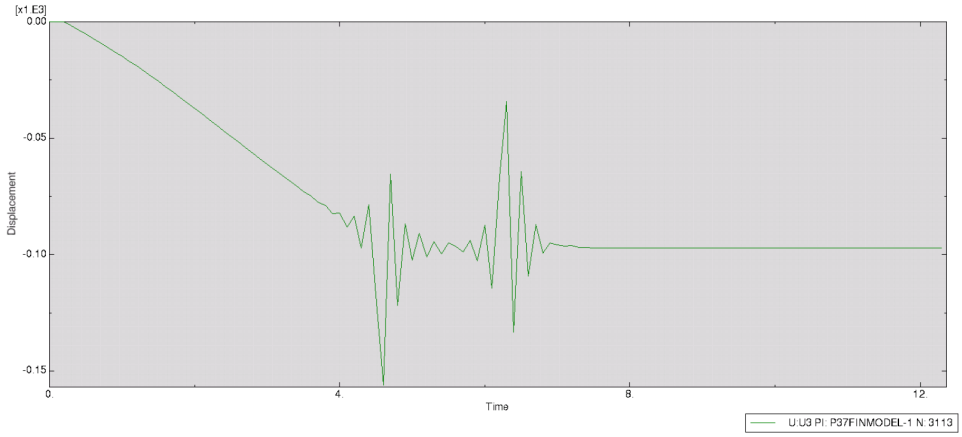

Figure 5.4: Displacement graph in ABAQUS

Star-ccm+ and with ABAQUS, which will be crucial to get data on the deflection and torsion of the fin.

In figures 5.5, there are presented two examples of post-processing images. On the left, the pressure field on the fin's surface is presented, being of paramount importance to understand the fin's behaviour during the FSI simulation. On the right the strain on the fin's inner surface is represented, allowing the user to know where the breaking points of the design are situated.

The pressure distribution on the fin is one of the most important results obtained from the flow field simulation, and will be used to compare the various simulations using both one-way and two-way FSI in chapter 6.

In this chapter, the coupling of both the CFD and FEA models into the FSI simulation was described. Having finalised the FSI model, the design tool is now complete and can be used in parametric studies to better understand the fin's behaviour.

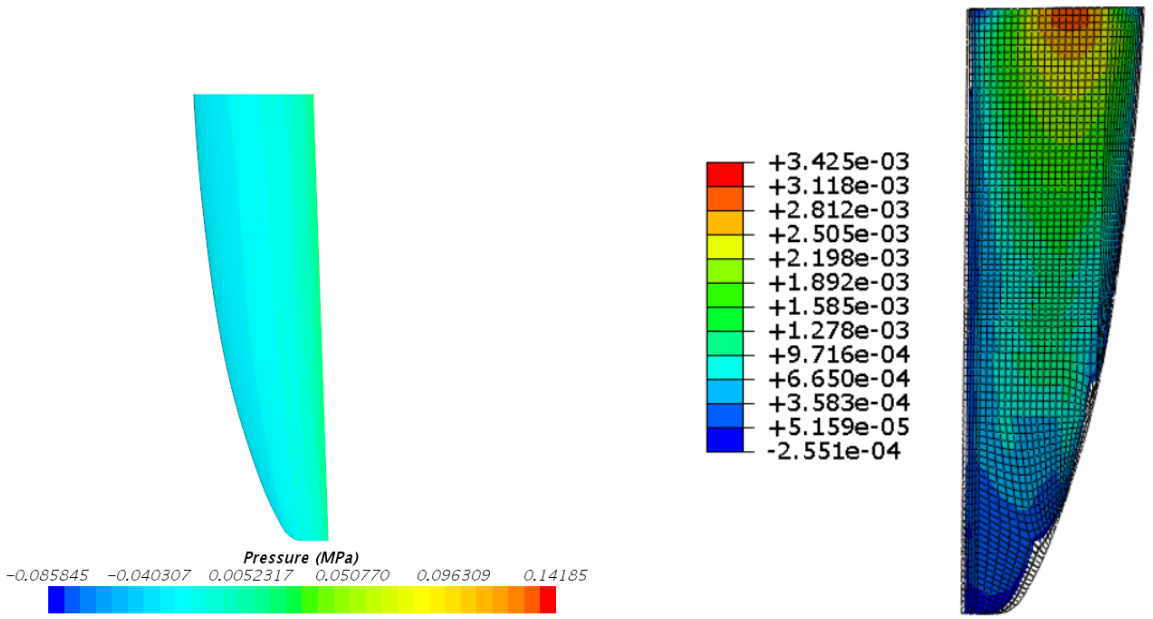

(a) Pressure field in the fin's outer surface-Star-CCM+

(b) Strain in the fin's inner surface, units in MPa -ABAQUS

Figure 5.5: Post-processing scenes for 25 knots and 2º AoA

Chapter 6

Parametric Study

Having developed the design tool, a parametric study was done to study the influence of certain input parameters on the behaviour of the windsurf fin, as well as the tool's performance. The changed parameters were the speed and angle of attack. The speeds chosen are standard velocities for a slalom windsurf. Ranging from 10 knots to 35 knots, with 35 knots being close to the design limit of the slalom windsurf fin. The angles of attack from 2 to 6 degrees are also thought to be typical of leeway angles experienced when windsurfing, where stall does not occur. A special case study was done into the 8 degrees, to test the design tool in stall conditions. Overall, over 7500 computational hours were spent during this parametric study.

- Speed : 10, 15, 20, 25, 30, 35 (knots)
- Angle of attack: 2, 4, 6, 8 (degrees)

The main aspects of the simulation that will be studied and analysed, from which conclusions will be taken from are:

- Lift Force
- Fin Deflection
- Fin Twist
- One-way vs two-way coupling

The Lift Force is a important hydrodynamic parameter, which corresponds to the force acting on the fin perpendicular to incoming flow, this is what the fin is designed to do. Fin deflection and twist are related to the fin structural response to the surrounding fluid loads. These two parameters change various behaviours like stall occurrence, the vertical lift forces and, most importantly, the controllability of the fin. They are often coupled together, as the bend-twist effect, which will be noticeable due to the large influence the twist has on the deflection and vice-versa. Despite the coupling between deflection and twist being highly influential on the fin performance, this behaviour is not fully understood yet. This study is an attempt at improving the knowledge on this phenomenon. Finally, the difference between one-way

and two-way FSI coupling is studied. This is a very important result of this study, because it allows the user of the design tool to know if the use of the two-way coupling is worth the extra computational cost relative to the faster, but less accurate, one-way coupling. The one-way coupling was done by analysing the fluid around the initial rigid undeformed body, therefore calculating the pressure field around the fin. These fields were then exported into ABAQUS, where they were inputted as a loading force on the fin. Finally, the response of the fin to these new loads was calculated and the deflection and twist of the fin's tip was analysed. Two-way coupling was done by using the design tool developed that was mentioned in chapter 5.

6.1 Lift Force

The lift force here evaluated is the most significant hydrodynamic force acting on the fin. It is the component of the resultant force, which is perpendicular to the incoming flow direction. When steadily sailing without accelerating nor curving, the fin's lift forces balance with the aerodynamic side force acting on the sail. For all the simulations studied, the lift force was calculated in Star-CCM+. The lift force calculation is possible by knowing the pressure distribution along both surfaces of the fin. The lift force is the vector sum of the pressure times the surface area around the entire fin. In other words, the surface integral of the pressure along the fin's surface area.

$$\vec{L} = \int P d\vec{A} \tag{6.1}$$

For each sailing condition studied, or pair of speed and angle at attack, a one-way and a two-way FSI analysis was done, results of which appear in figure 6.1.

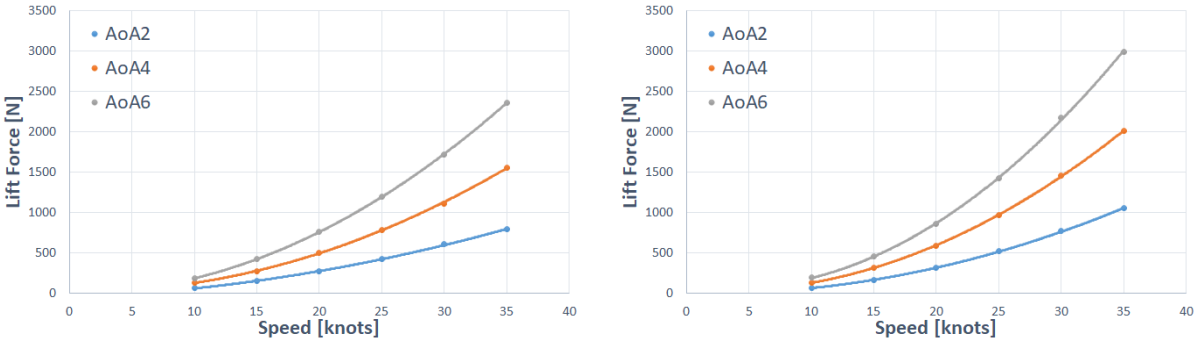

(a) Lift vs speed for one-way FSI

(b) Lift vs speed for two-way FSI

Figure 6.1: Lift vs speed for all operating conditions

Examining figure 6.1, it is clear and expected the increase of the lift force with both the velocity and the angle of attack. As for the angle of attack, as was seen before in subsection 2.5.2, a higher angle of attack often means a higher lift coefficient, which was confirmed by the results of the simulations in both one-way and two-way FSI.

Observing figure 6.2, it can be clearly seen that the lift coefficient increases with the angle of attack, confirming the theory. It is also obvious that two-way FSI represents a bigger increase in lift coefficient

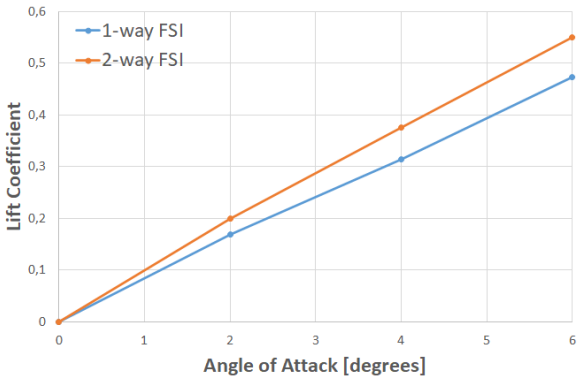

Figure 6.2: Lift Coefficient vs AoA

than one-way FSI. This phenomenon will have direct consequences in the lift force obtained by each analysis, since the lift force depends directly on the lift coefficient, as can be seen in equation 6.2. Where L is the lift force, C_L the lift coefficient, ρ the fluid's density, V the flow's velocity and A the surface of the wing, in this case, the fin.:

$$L = C_L \frac{1}{2} \rho V^2 A \tag{6.2}$$

From the previous graphs, it can also be seen that the lift force follows a parabolic path with the increasing velocity, in both one-way and two-way FSI. This is also supported by the theory, represented here in the equation above, that states that the lift force is directly proportional to the lift coefficient, a constant coefficient dependent on the profile, and has a quadratic response to the increasing velocity.

Since both FSI analysis seem to confirm the theoretical analysis, a comparison between the two seems necessary to withdraw any conclusions.

From figure 6.3, it is possible to compare the results using both methods of FSI. It is clear that while the fin's behaviour is similar, using two-way FSI results in higher lift forces overall, which means that the one-way coupling underestimates the fin's lift force response to the incoming flow.

The difference seems to increase with the speed, up until 35 knots, where the difference in lift plateaus, which is understandable given its near the limit for the windsurf fin and an unrealistic condition for a windsurf board. At the same time, the relative difference between the results seems to be independent from the angle of attack, meaning that the relative error does not change with an increase or decrease in AoA. The difference reaches a maximum of 33% for 35 knots at an AoA of 2º and a minimum of 3.7% for 10 knots at an AoA of 4º.

Observing the results of this comparison, it can be seen that as the relative error between the two coupling modes increases, it becomes too big to ignore. Therefore a compromise must be done between the accuracy of the results and computational costs. Defining the two-way FSI as the accurate analysis and expecting a relative error under 5%, there are only two operating conditions where the one-way FSI analysis meets this criteria. This is the case for the velocity of 10 knots, with an AoA of 2 and 4 degrees. In all other sailing conditions, the relative error is not worth the savings in computational costs or time. In Appendix B.1, the results for all operating conditions can be found. The lift forces for both analysis

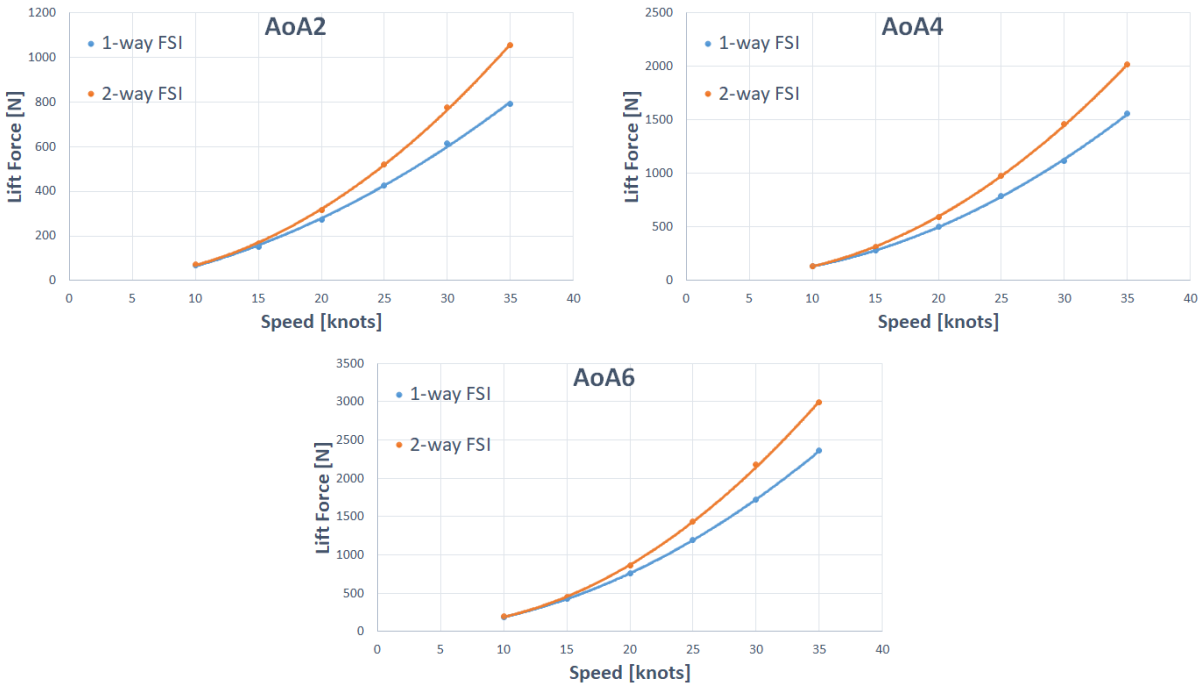

Figure 6.3: Lift force comparison between one-way and two-way FSI

models, as well as, the relative errors are presented.

In conclusion, the two-way FSI analysis is significantly more accurate and should be used for almost all simulations, in order to get a good grasp of the material behaviour in movement. Important findings are summarized below:

- Lift force increases with both speed and angle of attack for both FSI models
- Two-way FSI increases lift force compared to one-way FSI
- Difference between both models indicates that it is useful to use two-way FSI in almost all simulations

6.2 Fin Deflection

Deflection is a natural behaviour of a cantilever type structure clamped at one end and loaded along its surface. In the particular case of this thesis, the windsurf fin is fixed by the base to the board and the pressure loads are hydrodynamically induced by the surrounding flow. In all simulations here presented, load oscillations and the dynamic study of natural frequencies were disregarded.

The deflection was calculated at the tip of the fin, since this will be the most deformed point of the structure and was compared with the initial undeformed rigid structure, as can be seen in figure 6.4. As mentioned previously, the deflection will be calculated by ABAQUS, with the pressure loads imported from Star-ccm+, where they were calculated, to the fin's surface.

It is easily observable in figure 6.5, that the tip deflection follows the same pattern as the lift force previously, increasing with both speed and angle of attack. This makes sense, since the lift force is a

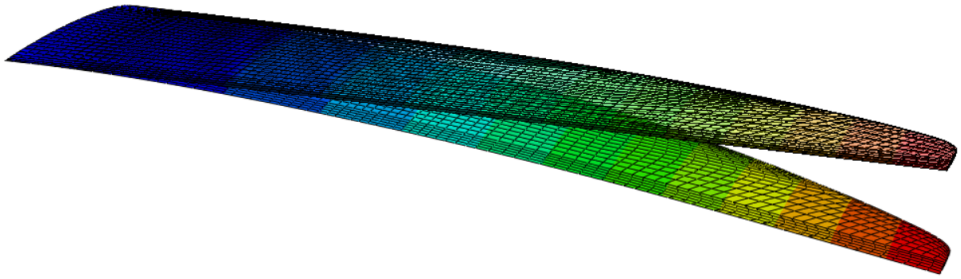

Figure 6.4: Deflection and undeformed geometry of the fin at 10 knots and 6º AoA

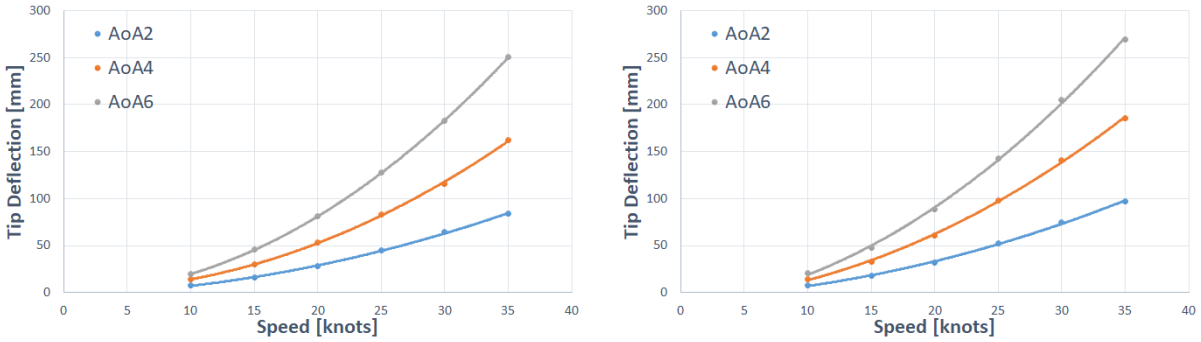

(a) Tip Deflection vs speed for one-way FSI

(b) Tip Deflection vs speed for two-way FSI

Figure 6.5: Tip Deflection vs speed for all operating conditions

translation of the pressure loads into a single vector, and, as said above these pressure loads are the catalyst for the fin's deflection.

Similarly to the previous section, lift force analysis, a comparison between both methods of FSI is needed to withdraw any conclusions, so all operating conditions were simulated using both methods.

A comparison between the numerical results obtained by using the Multiple Iteration FSI model and using the simplification of a single iteration analysis is possible. For every condition analysed, a significant difference is clear between the "1-way FSI" and "2-way FSI" results, being the results obtained by the single iteration simplification method ("1-way FSI") always lower than the multiple iteration ones. This means that simplifying these simulations by not using the automated FSI model, will again, similarly to the lift force results, under-estimate the maximum tip deflection.

The relative error between one-way and two-way FSI drops significantly, when compared to the lift force graphs, as can be seen in figure 6.6. The difference increases for higher speeds, reaching a maximum of 21.6%, for 30 knots at an AoA of 4º, and with a minimum value of 2.5%, for 10 knots at an AoA of 2º.

Another conclusion that can be taken is the fact that this discrepancy is highly influenced by the speed but not so much by the angle of attack, meaning that there is not a clear correlation between the error and the angle of attack.

As previously said in section 6.1, a compromise must be done between result accuracy and computation time, therefore a decision must be taken regarding the use of the two-way FSI model or not. Applying the same standard used for the lift force analysis, of a 5% margin of error, only three operating

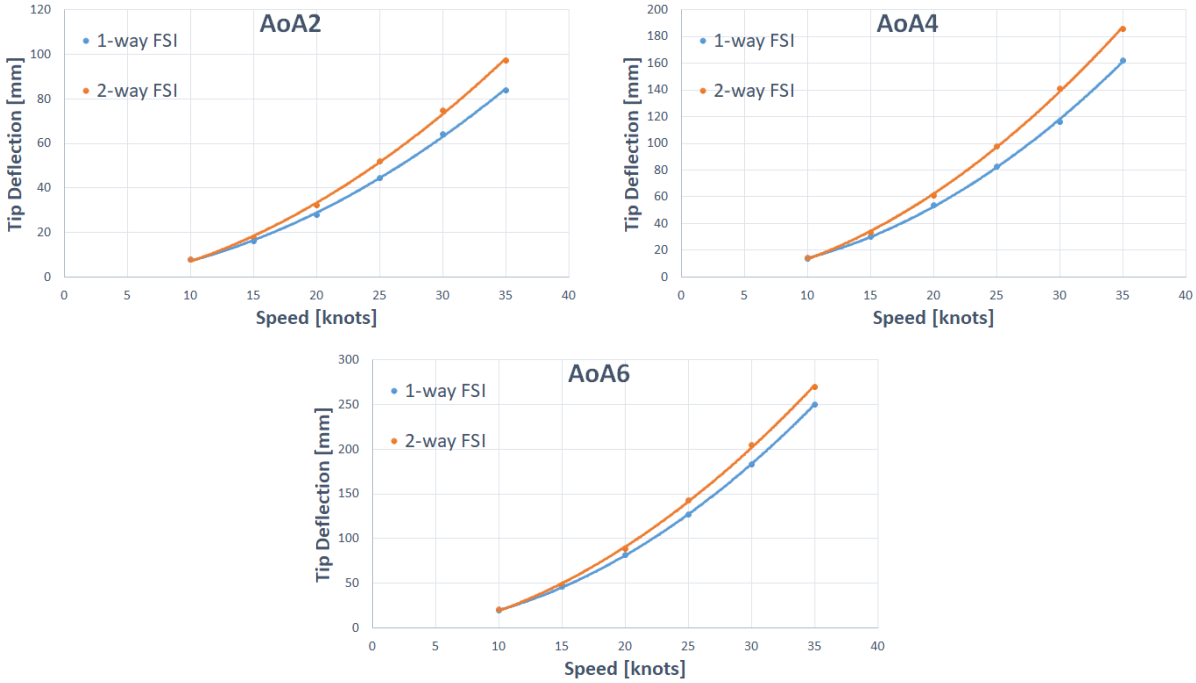

Figure 6.6: Tip Deflection comparison between one-way and two-way FSI

conditions meet the criteria. Both of the previous accurate conditions for lift force, velocity of 10 knots with an AoA of 2 and 4 degrees, as well as one with an AoA of 6 degrees, sailing at 15 knots. Overall, the errors are too large to ignore, hence it is recommended to use the multiple iterations FSI using the tool developed.

In Appendix B.2, the results for tip deflection are presented for all the conditions studied during this project. The deflections presented refer to the results obtained from both methods, along with the respective relative errors.

The deflection distribution throughout the fin, seen in figure 6.7, is a very important aspect of this parameter, because it shows the user if the fin is behaving as expected. In this case, the deflection increases as the points are further away from the root, where the fin is attached to the board, reaching its maximum point at the fin tip. This was the expected result, due to the cantilevered condition set at the root, the image also shows that the deflection is close to parallel to the root, which make sense in a low twist case like the one represented.

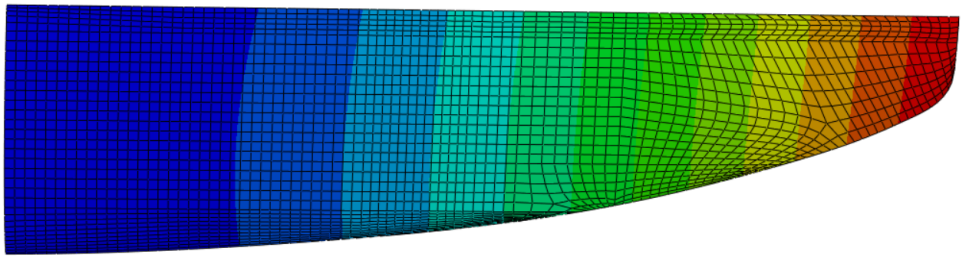

Figure 6.7: Deflection distribution of the fin at 10 knots and 6º AoA-2-way FSI

The most important findings are summarized here:

- Fin deflection increases with both velocity and angle of attack for both FSI models
- Two-way FSI increases fin deflection compared to one-way FSI
- Difference between both models indicates that it is useful to use two-way FSI in almost all simulations

6.3 Fin Twist

The twist parameter, similarly to the deflection, is a natural structural behaviour of the fin when it is being pressure loaded along its surfaces. Contrarily to the previous two parameters studied, twist is very sensitive to small changes in the domain characteristics, which means that it is expected for the value to fluctuate more than lift force and tip deflection. Physically, this can be explained due to small differences in the pressure distribution around the fin, generation of separation bubbles on the boundary layer and the small dimensions of the fin's tip (around 23 mm of chord and maximum thickness of 2 mm). All of these phenomenona are sufficient to alter the tip twist, while not being sufficient to change the lift force and tip deflection. Because of this, tip twist was not one of the main convergence parameters opposed to the former two, and this will be clear in the results obtained.

In figure 6.8, all twist angle solutions are displayed for both methods. A positive twist angle was defined as one that increases the angle of attack seen by the fin's tip relative to the fluid flow.

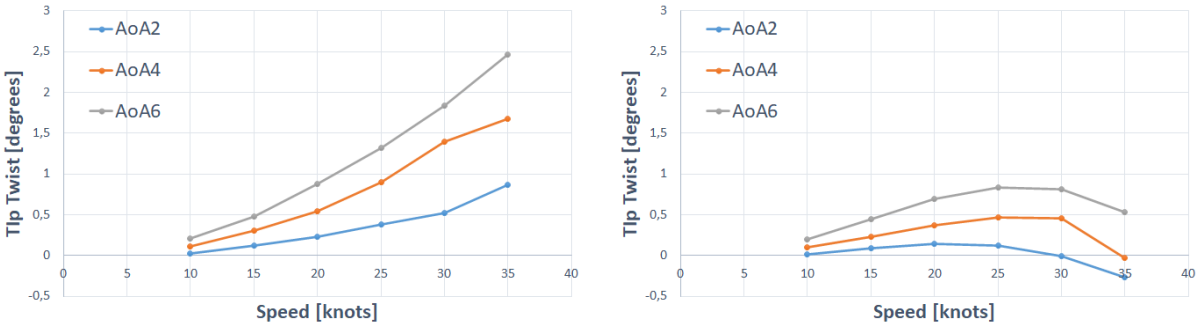

(a) Tip Twist vs speed for one-way FSI

(b) Tip Twist vs speed for two-way FSI

Figure 6.8: Tip Twist vs speed for all operating conditions

Analysing figure 6.8, two different sets of behavior can be seen. One is related to the one-way FSI method, where overall the tip twist increases with the increase of speed, as well as the angle of attack. In the other set of solutions, for two-way FSI, values in general are much lower when compared to the one-way FSI, they seem to increase with speed and angle of attack until a certain point where the increase in speed induces a decrease in the angle of twist.

For one-way FSI, the increase of twist angle with speed and angle of attack seem to agree with previous results for lift force and tip deflection. This increase in angle of twist translates, as was mentioned above, into an increase of the angle of attack of the fin's tip, which subsequently should increase the lift force and tip deflection in the next iterations. This was seen in the previous results, where the two-way FSI, with multiple iterations, increased both of those parameters with speed and angle of attack.

In the two-way FSI model, the results show a behaviour that is hard to explain without more data, therefore further examining into these results is necessary.

In figure 6.9, both models are compared with each other for each sailing condition, in order to further understand the fin's behaviour. In appendix B.3, the results for the fin's tip twist are presented, for all operating conditions alongside the respective relative errors.

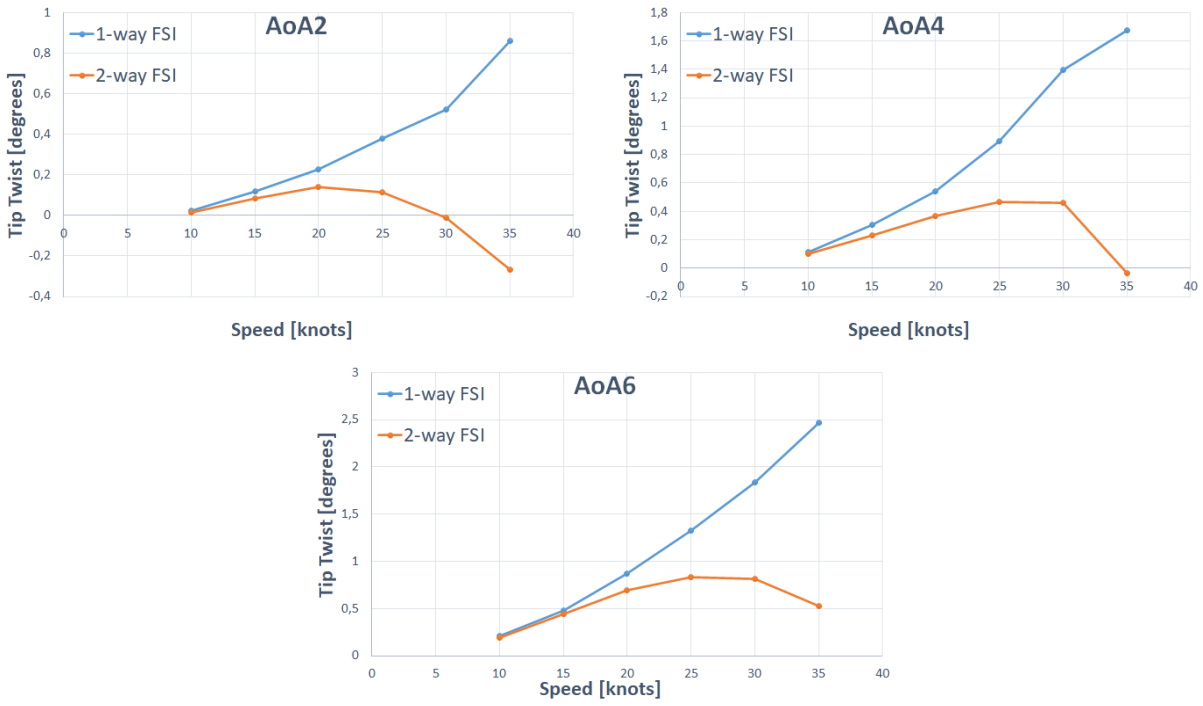

Figure 6.9: Tip Twist comparison between one-way and two-way FSI

Looking at figure 6.9, it is further obvious the difference between the prediction of the fin behaviour for each model. While the one-way FSI clearly predicts an increase in the twist with the increases of both speed and angle of attack, as was noticed before, the two-way FSI predicts a low angle of twist across all operating conditions, making the single iteration method a clear over-prediction. It can also be seen that the gap between both values increases with the increase in speed across all AoA. This pattern can also be seen in section B.3, despite the relative error not having the same behaviour, due to very small numbers of twist in some cases. With this difference in mind, it is clear that more research has to be done, especially investigating why the twist behaves as it does in each model, and what is the fin's behaviour throughout the multiple iterations of the two-way FSI that leads to the final results.

The twist of a composite aerofoil shaped structure, like the fin, may come from two main effects: the hydrodynamic forces on the fin's profile and twisting moments resulting from bending moments due to the coupling between these two effects.

The hydrodynamic forces acting on the fin's profile may cause a pitching moment considering that the elastic axis of the fin does not coincide with the pressure centre (point at which the hydrodynamic forces are applied). Considering that the fin is not a 2D aerofoil but a finite wing, with a non-constant chord and is built from composite materials, this pitching moment should exist. It is however very difficult to determine the location of these points, and due to that, difficult as well to determine this moment.

Therefore it falls out of the scope of this work.

The coupling between bend and twist can come from three main effects as discussed in section 2.4. In this fin the effect most likely to be more dominant is the effect due to the shape of the fin, particularly, having a 2 ° rake to the aft. Given that the ply layup is totally symmetric and therefore should give no bend-twist coupling by itself if perfectly applied.

A combination between these effects appears to be the origin of the difference between the one-way FSI and the two-way FSI, with no clear indicator as to which one is the predominant one without further work.

6.3.1 Two-way FSI iteration analysis

Further research into the twist behaviour, during the multiple iterations, was done. Figure 6.10 shows the evolution of the twist angle throughout the multiple iterations needed for the two-way FSI to reach a reliable result. Two cases are here analysed, one with a smaller difference in angle of twist, the 25 knots cases, and one with a bigger gap, the 35 knots case.

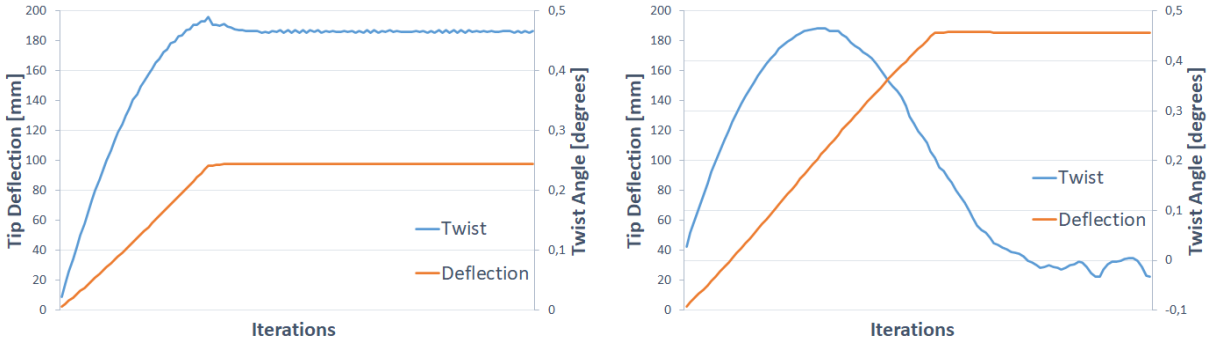

(a) Twist angle and deflection evolution through iterations (V25 AoA4)

(b) Twist angle and deflection evolution through iterations (V35 AoA4)

Figure 6.10: Twist angle and deflection evolution through iterations

In these graphs, a more familiar pattern emerges. While the deflection and the lift force are increasing, due to numerical ramping, both parameters have the same behaviour, the twist angle increases similarly to the one-way FSI model. However, once the deflection reaches a value closer to its final value, or equilibrium state, the twist seems to have two different responses, one for lower velocities and one for higher velocities.

In low velocity cases, the twist stabilizes at an angle close to its maximum value, seen just before the deflection converges. However, at higher velocities, the twist decreases dramatically after this maximum value for all angles of attack, as illustrated in figure 6.10 on the right. One possible explanation to this sudden drop in twist angle may be the appearance of separation bubbles during the FSI iterations, which dissipate as the flow field reaches a final state. In order to investigate this assumption, the flow field after one iteration of two-way FSI, was compared with the flow field at the end of the multiple iteration FSI, as shown in figures 6.11 and 6.12.

In figure 6.11, for 25 knots, there does not appear to be any big difference between the two fields

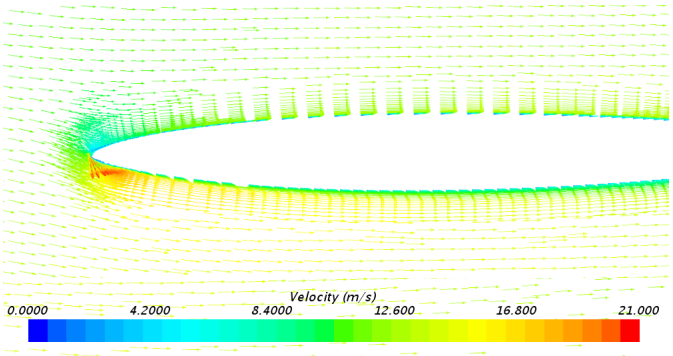

(a) Velocity field after one iteration (V25 AoA4)

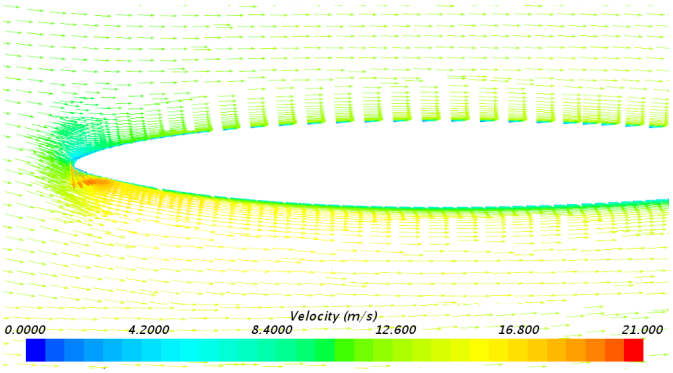

(b) Velocity field after two-way FSI (V25 AoA4)

Figure 6.11: Velocity fields for 25 knots and 4 AoA

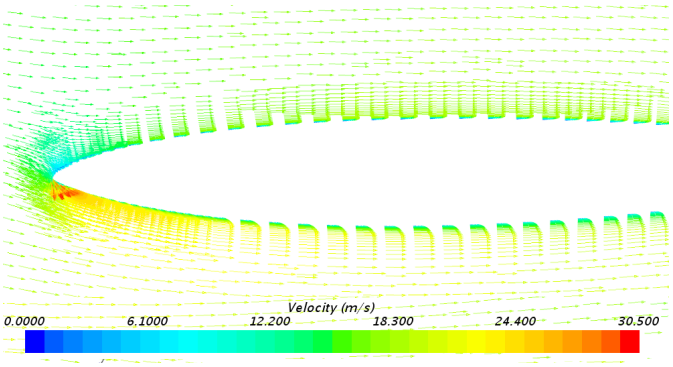

(a) Velocity field after one iteration (V35 AoA4)

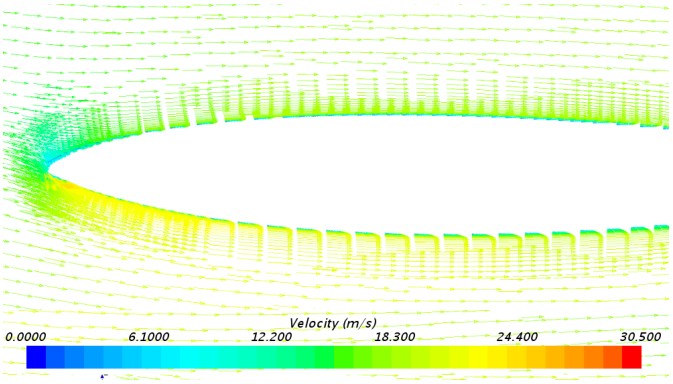

(b) Velocity field after two-way FSI (V35 AoA4)

Figure 6.12: Velocity fields for 35 knots and 4 AoA

displayed. This corroborates the twist angle results, since the twist angle after numerical ramping, is very similar to the final twist value. However, in figure 6.12, for 35 knots, differences in velocity near the leading edge can be seen between the two plots. This difference in velocity can be explained by a bigger angle of attack after one iteration than in the final step. This result confirms the difference between the one-way FSI and the two-way FSI simulations, however it does not present meaningful data to explain why this behavior occurs. This analysis of the velocity field can be confirmed by the pressure fields around the fin in both sections, represented in figures 6.13 and 6.14.

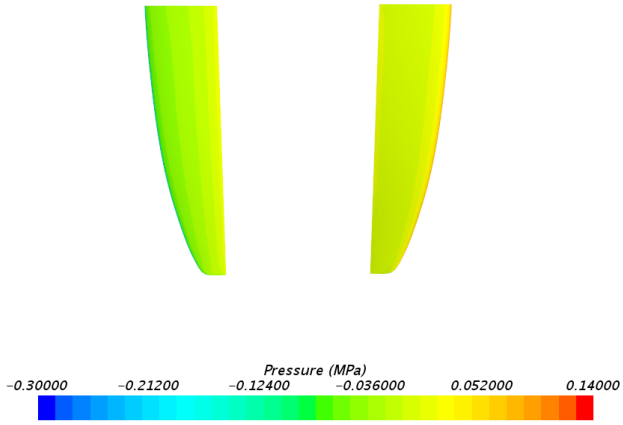

(a) Pressure field after one iteration (V25 AoA4)

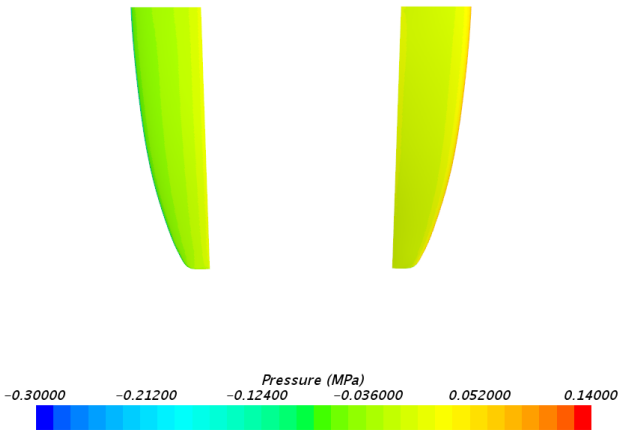

(b) Pressure field after two-way FSI (V25 AoA4)

Figure 6.13: Pressure fields for 25 knots and 4 AoA

In figure 6.13, no clear difference is seen in both fields, which again confirms that the twist angle is very similar. In figure 6.14 a difference can be seen in the pressure fields of both sides of the fin, with a slightly lower pressure in the leading edge of the ”upper surface”, in this case left-side surface, and a higher pressure in the leading edge of the ”lower surface”, in the fin’s case right-side surface, in the one iteration simulation. This bigger gap in the pressure difference is the reason for the higher velocity on the one iteration FSI, seen in figure 6.12. Another behaviour that can be observed, from the pressure fields is that there seems to be no loss of pressure due to vortex effect, which is common in finite wings.

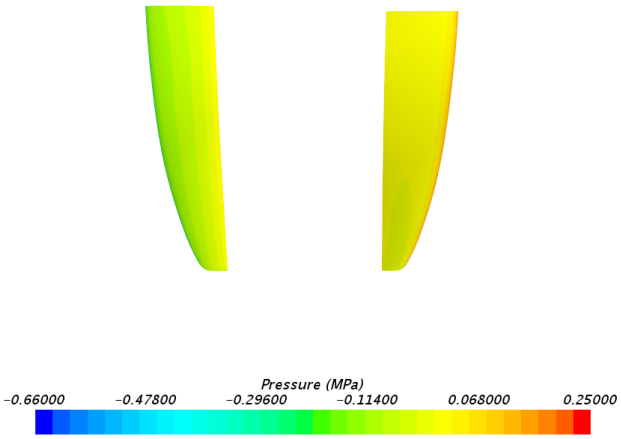

(a) Pressure field after one iteration (V35 AoA4)

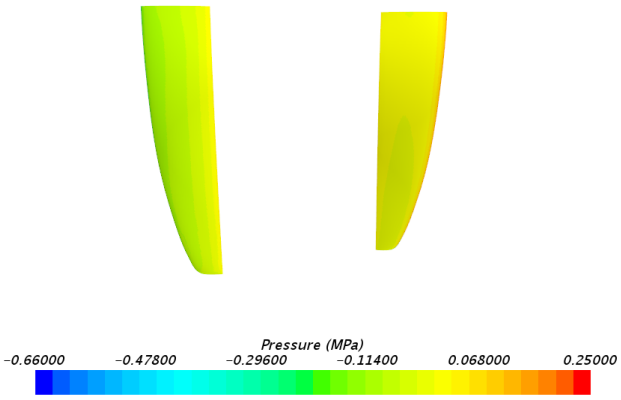

(b) Pressure field after two-way FSI (V35 AoA4)

Figure 6.14: Pressure fields for 35 knots and 4 AoA

It appears that the deflection of the fin acts as a winglet, stopping the high pressure field from the lower surface from escaping into the upper surface.

In appendix B.4, pressure fields for 15, 25 and 35 knots and all angles of attack are presented, confirming the difference in the flow fields between the simple CFD study with a rigid fin and the multiple iteration FSI.

Overall, the multiple iteration FSI leads to a decrease of the angle of twist, when compared with the single iteration FSI, with very small angles of twist across all operating conditions. Using the same criteria as before, although the low velocity cases seem to have very similar angles of twist, the relative difference between results is larger than 5%. Therefore the multiple iteration FSI should be used for all simulation conditions. Most significant findings regarding fin twist are summarized here:

- Fin twist increases with both velocity and angle of attack for one-way FSI
- Fin twist for two-way FSI is generally low, reaching negative angles for some conditions
- Two-way FSI decreases fin twist compared to one-way FSI

- There are two main effects responsible for the fin twist: bend-twist coupling due to the specific lay-up of the anisotropic composite materials used, which decreases the twist, and pitching moment due to the force applied on the fin, which increases the twist
- Two-way FSI should be used for all operating conditions

6.4 Case study: Stall

Finally, to investigate the influence of a separation bubble on the FSI model, a single test with 8 degrees of AoA at 20 knots was done.

Figure 6.15 shows the velocity field around the fin at 10 centimeters from the root of the fin, with vectors defining the velocity's direction and the scalar value colour coded. As shown in figure 6.15, a laminar separation bubble appears near the leading edge of the suction surface of the fin, on both the simple CFD around the rigid fin and in the two-way FSI model. The multiple iteration method seems to predict a slightly higher velocity near the leading edge than the simple CFD method, which makes sense since the effective angle of attack is higher due to the positive twist angle in the two-way FSI model.

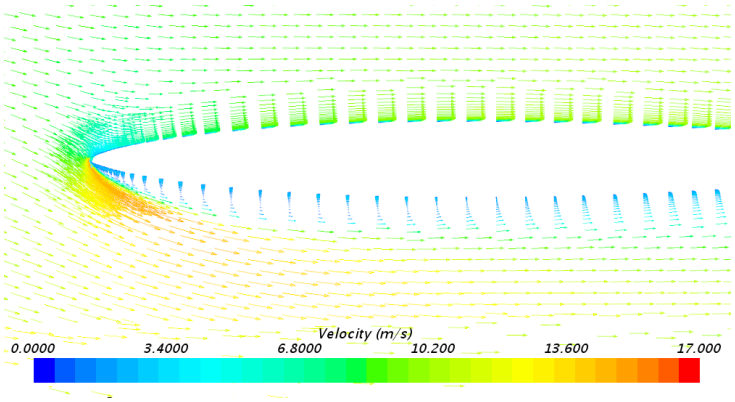

(a) Velocity field for the rigid fin (V20 AoA8)

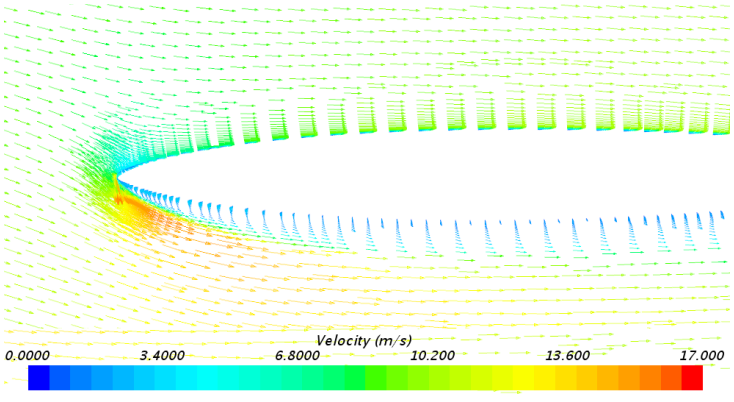

(b) Velocity field after two-way FSI (V20 AoA8)

Figure 6.15: Velocity fields for 20 knots and 8 AoA

Figures 6.16 not only show the pressure around the fin, but also show the wall shear stress isolines. Two different behaviours of these isolines can be seen, in the suction surface the lines are sometimes perpendicular to the flow direction, this indicates where the turbulent flow reattaches to the fin's surface

after a separation bubble. On the other side of the fin, the pressure or lower surface, the lines are parallel to the flow's direction, which indicates that the flow does not separate.

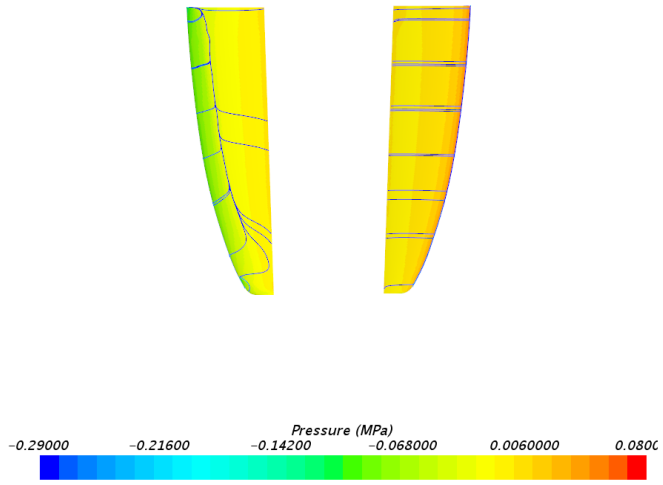

(a) Pressure field for the rigid fin (V20 AoA8)

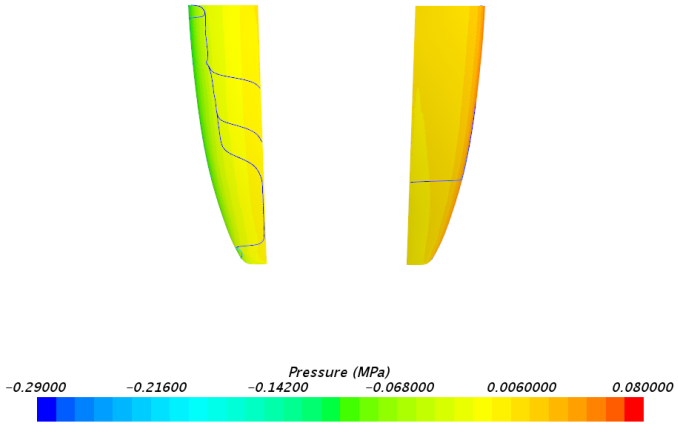

(b) Pressure field after two-way FSI (V20 AoA8)

Figure 6.16: Pressure fields for 20 knots and 8 AoA

Some differences are observable when comparing the FSI results of this case with a laminar separation bubble with all the other previous cases. For all previous operating conditions, the deflection was greater for the multiple iteration method, but since here the fin has stalled, the same behaviour is not expected. As previously described, when a airfoil enters stall, its ability to produce lift decreases significantly. In fact, the deflection is approximately the same here for both methods, the 2-way value being 2.5% less than the one-way value. Similarly, the increase in lift force from one-way to two-way solutions was small (4.1%) compared with previous, non-stalled, scenarios. However, twist angle change between 1-way and 2-way solutions was similar to that for non-stalled operation, decreasing from 1.23 degrees to 0.86 degrees.

The differences in behaviour seen for this stalled case compared to the previous cases both confirms that an AoA of 8 degrees would not occur under regular sailing conditions, and also gives confidence

that the model behaves as expected even under extreme conditions.

Chapter 7

Conclusions

The main objective of this Thesis was to develop an integrated fluid-structure interaction analysis model, in order to have a more accurate knowledge of the behaviour of the fin in operation.

The biggest challenge faced during the course of this work was the scarcity of accurate data regarding the FSI process. This led to a process of trial and error regarding the development of the FEA model and the CFD model, in order to have suitable models ready to communicate with each other.

7.1 Achievements

The main achievements of this project were the selection of the material properties to do the structural study, the generation of a finite element analysis model in ABAQUS, the development and improvement of a computational fluids dynamic model in Star-ccm+ and perfecting the coupling process between FEA and CFD into a fluid-structure interaction model. The FSI model created is a multiple iteration, automated FSI model which is easy to use and can be applied easily in other applications and parametric studies.

Further, valuable new information concerning the behaviour of the fin in operation, taking into account hydro-elastic effects, was obtained. In particular, three parameters were studied in depth: the fin's lift force, the fin's tip deflection and the fin's tip twist.

A solid understanding of the response of the lift force and the tip deflection in operating conditions was achieved, both of which increased with the increase in speed and angle of attack, and were higher for the two-way FSI when compared to the one-way FSI model.

The behaviour of twist was not as simple, and hence required further research regarding its evolution throughout the multiple iterations of the model. Two main effects causing twist angle were identified: bend-twist coupling of the composite material and pitching moment. The influence of these two effects was isolated and it was found that the bend-twist coupling led to a decrease in the angle of twist, while the pitching moment increased the twist. Overall, a lower twist was predicted by the multiple iteration FSI model than was by the one-way FSI.

Finally, the study of a operating situation with 8 degrees of angle of attack was done, in order to investigate stall conditions. As expected, stall condition was achieved for 20 knots with 8 degrees AoA,

and the output results changed accordingly, with the lift force and tip deflection not changing compared to one-way FSI, while fin's tip twist maintained the same behaviour, decreasing compared to one-way FSI.

It was found that the two-way FSI model improves the results across all operating conditions and, therefore, should be used in any analysis of the fin's behaviour while in operation.

7.2 Future Work

The work completed during this Thesis contributes as one of the final steps of a continuous work around a slalom windsurf fin, with the objective of creating the technology capable of constructing a fin that behaves exactly as desired. The design tool built in this Thesis is very powerful and can be used in future studies with the goal of better understanding the windsurfer fin. Some of the studies possible and the improvements required are:

- Developing a parametric study using ply placement, composition and orientation as inputs to check the alteration on the fin's behaviour;
- Studying the percentage of carbon fibres that can be substituted for glass fibres, in order to save costs, while maintaining an acceptable stiffness;
- After improving the FEA model by including strength analysis, doing a parametric study regarding which operating conditions can be achieved without fracturing of the fin;
- Improving the replication of the fin's layup by trying different positioning for the plies, which could alter the bend-twist coupling, and observe the alteration on the fin's behaviour;

Bibliography

[1] J. Graham-Jones and J. Summerscales. *Marine Applications of Advanced Fibre-reinforced Composites*. Woodhead Publishing, 1^{st} edition, 2015.

[2] S. Selvaraju and S. Ilaiyavel. Applications of composites in marine industry. *Journal of Engineering Research and Studies*, 2(2):89–91, 2011.

[3] R. Shenoi and J. Wellicome. *Composite Materials in Maritime Structures, Volume 1 Fundamental Aspects*. Southampton, 1^{st} edition, 1993.

[4] F-HOT. F-HOT RWS SLALOM FINS, 2020. URL http://www.f-hot.com/fins (January 2021.

[5] K. Ismail. The hydrodynamic theory of vertical swept hydrofoils near a free surface and comparison with measurement. *PhD Thesis, University of Southampton*, 1973.

[6] H. E. Saunders. *Hydrodynamics in Ship Design, Volume 3*. The Society of Naval Architects and Marine Engineers, 1^{st} edition, 1957.

[7] J. D. Anderson. *Computational Fluid Dynamics: The Basics with Applications*. McGraw-Hill, 1^{st} edition, 1995.

[8] C. Broers, T. Chiu, M. Pourzajani, and D. Buckingham. Effects of fin geometry and surface finish on sailboard performance and manoeuvrability. *Manoeuvring and Control of Marine Craft*, pages 275–289, 1992.

[9] T. Chiu, T. Van den Bersselaar, C. Broers, and D. Buckingham. The effect of tip flexibility on the performance of a blade type windsurfer fin. *Manoeuvring and Control of Marine Craf*, pages 261–274, 1992.

[10] S. Fagg and X. Velay. Simulating the operation of a novel variable camber hydrofoil. In *1996 IEEE Aerospace Applications Conference. Proceedings*, volume 3, pages 261–271, Aspen, CO, USA, 1996.

[11] S. Fagg. *The development of a reversible and finitely variable camber windsurf fin*. PhD thesis, Bournemouth University, 1997.

[12] A. Kunoth, M. Schlichtenmayer, and C. Schneider. Speed windsurfing: Modeling and numerics. *International Journal of Numerical Analysis and Modeling*, 4(3-4):548–558, 2007.

[13] M. Findlay and S. Turnock. Investigating sailing styles and boat set-up on the performance of a hydrofoiling moth dinghy. In *20th International HISWA Symposium on Yacht Design and Yacht Construction, Delft*, November 2008.

[14] C. Lothode, M. Durand, Y. Roux, A. Leroyer, M. Visonneau, and L. Dorez. Dynamic fluid-structure interaction of a foil. In *INNOV'SAIL 2013*, June 2013.

[15] L. M. Giovannetti. Fluid structure interaction testing, modelling and development of passive adaptive composite foils. *Ph.D. Thesis, University of Southampton*, 2017.

[16] L. S. Sutherland. Windsurfer fin hydrodynamics. *Master's Thesis, University of Southampton*, 1993.

[17] F. A. M. R. Nascimento. Windsurf fin - numerical and experimental analysis of ultimate strength. *Master's Thesis, Instituto Superior Técnico*, 2017.

[18] E. Balzer. Development of a design tool for investigating lay-up schedule designs of a composite windsurfer fins. *Master's Tthesis, Instituto Superior Técnico*, 2018.

[19] A. M. R. dos Santos. Hydrodynamic analysis of a slalom fin of windsurf board. *Master's Thesis, Instituto Superior Técnico*, 2018.

[20] A. R. Q. Saldanha. Hydrodynamic and fluid-structure interaction analysis of a windsurf fin. *Master's Thesis, Instituto Superior Técnico*, 2019.

[21] Guide to composites. Technical Report GTC-6-0417, Gurit, 2020.

[22] L. Sutherland. A review of impact testing on marine composite materials: Part I – marine impacts on marine composites. *Composite Structures*, 188:197–208, March 2018.

[23] B. Veritas. Raw materials for laminates. *Hull in Composite Materials and Plywood, Material Approval, Design Principles, Construction and Survey*, 2018.

[24] ANSYS©. Ansys inc, 2020. Cannonsburg, PA, USA,.

[25] R. Jones. *Mechanics of Composite Materials*. Taylor & Francis, 2^{nd} edition, 1999.

[26] J. Cherusseri, S. Pramanik, L. Sowntharya, D. Pandey, K. K. Kar, and S. D. Sharma. *Composite Materials:Processing, Applications, Characterizations*. Springer, 1^{st} edition, 2017. ISBN:978-3-662-49514-8.

[27] J. Martin. *Materials for Engineering*. Woodhead Publishing, 3^{rd} edition, 2006. ISBN:9781845691578.

[28] L.Vignoli, M.Savi, and P.M.C.L.Pacheco. Comparative analysis of micromechanical models for the elastic composite laminae. *Composites Part B*, 2019.

[29] A. Altmann. Strength prediction of ply waviness in composite materials considering matrix dominated effects. *Composite Structures*, 2015.

[30] E. J. Barbero. *Finite Element Analysis of Composite Materials using Abaqus*. CRC Press, 1^{st} edition, 2013. ISBN:978-1-4665-1663-2.

[31] Abaqus simulia, abaqus analysis user's guide, 2013.

[32] S. Rohde, P. Ifju, B. Sankar, and D. Jenkins. Experimental testing of bend-twist coupled composite shafts. *Experimental Mechanics*, 55, 07 2015.

[33] . `https://en.wikipedia.org/wiki/File:Wing_profile_nomenclature.svg` (March 2021).

[34] . `http://bandung-aeromodeling.com/tutorial.php?nid=51&like=1` (March 2021).

[35] C.S.Smith. *Design of Marine Structures in Composite Materials*. Elsevier Ltd., 1^{st} edition, 1990. ISBN:978-1851664160.

[36] S.Sleight. *Modern Boat Building: Materials and Methods*. Conway Maritime Press Ltd., 1^{st} edition, 1985. ISBN:978-1851664160.

[37] M.H.Sharqawy, J. H. Lienhard, and S. M. Zubair. Thermophysical properties of seawater: A review and new correlations that include pressure dependence. *Desalination and Water Treatmen*, 2010.

[38] Star-CCM+. Star-ccm+ user guide, 2018.

[39] A. Marta. Lecture 08: Aerostructural analysis and optimization. lecture notes, Aircraft Optimal Design, IST, 2018.

[40] R. de Borst, P. Nithiarasu, T. Tezduyar, G. Yagawa, and T. Zohdi. *Computational Fluid-Structure Interaction*. John Wiley & Sons, Ltd., 2012. ISBN:9780470978771.

[41] F. Benra, H. Dohmen, J. Pei, S. Schuster, and B. Wan. A comparison of one-way and two-way coupling methods for numerical analysis of fluid-strcutrure interactions. *Journal of Applied Mathematics*, 2011.

[42] J. Donea, S. Guiliani, and J. Halleux. An arbitrary-lagrangian-eulerian finite element method for transient dynamic fluid-structure interaction. *Computer Methods in Applied Mechanics and Engineering, Volume 33*, 1993.

[43] J. Sigrist. *Fluid-Structure Interaction an introduction to finite element coupling*. Wiley, 2015. ISBN:978-1119952275.

Appendix A

ABAQUS Code

The input file for the FEA analysis needs to be changed in order to be able to communicate with Star-CCM+, this code is an example of those alterations.

A.1 Inputs for FSI simulation

*Co-simulation, name=”Co-simulation with STAR-CCM +”, program=MULTIPHYSICS
*Co-simulation Region, import
ASSEMBLY_P37FINMODEL-1_FIN, CF
*Co-simulation Region, export
ASSEMBLY_P37FINMODEL-1_FIN, U
*CO-SIMULATION CONTROLS, COUPLING SCHEME=ITERATIVE, SCHEME MODIFIER=LEAD, NAME=couplingsche
*CO-SIMULATION CONTROLS, STEP SIZE=0.1, NAME=stepsize

Appendix B

Numerical Results

B.1 Lift Force

The next tables show the lift force numerical results obtained by the simulations of the fin in all operating conditions. The results for the single iteration analysis, as well as the multiple iteration model are shown, along with the relative difference.

Table B.1: Lift Force numerical results at 2º AoA

Speed [knots]	Lift (2-way FSI)[N]	Lift (1-way FSI)[N]	Relative Difference [%]
10	72,58	69,68	4,00
15	167,58	152,65	8,91
20	315,11	273,54	13,19
25	520,81	426,90	18,03
30	774,78	614,03	20,75
35	1053,94	792,36	24,82

Table B.2: Lift Force numerical results at 4º AoA

Speed [knots]	Lift (2-way FSI)[N]	Lift (1-way FSI)[N]	Relative Difference [%]
10	135,70	130,89	3,55
15	317,72	280,18	11,81
20	593,83	506,33	14,73
25	975,72	789,42	19,09
30	1458,99	1116,74	23,46
35	2012,16	1560,80	22,43

Table B.3: Lift Force numerical results at 6º AoA

Speed [knots]	Lift (2-way FSI)[N]	Lift (1-way FSI)[N]	Relative Difference [%]
10	196,92	185,55	5,78
15	457,11	431,01	5,71
20	859,78	766,31	10,87
25	1428,40	1193,70	16,43
30	2175,55	1721,74	20,86
35	2994,23	2364,66	21,03

B.2 Tip Deflection

The next tables show the tip deflection numerical results obtained by the simulations of the fin in all operating conditions. The results for the single iteration analysis, as well as the multiple iteration model are shown, along with the relative difference.

Table B.4: Tip Deflection numerical results at 2º AoA

Speed [knots]	Tip Deflection (2-way FSI)[mm]	Tip Deflection (1-way FSI)[mm]	Relative Difference [%]
10	7,85	7,66	2,44
15	17,59	16,26	7,59
20	32,36	28,09	13,17
25	52,11	44,64	14,33
30	74,79	64,24	14,11
35	97,11	83,88	13,62

Table B.5: Tip Deflection numerical results at 4º AoA

Speed [knots]	Tip Deflection (2-way FSI)[mm]	Tip Deflection (1-way FSI)[mm]	Relative Difference [%]
10	14,45	14,04	2,87
15	33,29	29,81	10,46
20	61,06	53,57	12,26
25	97,69	82,79	15,25
30	141,05	116,00	17,76
35	186,01	162,09	12,85

Table B.6: Tip Deflection numerical results at 6º AoA

Speed [knots]	Tip Deflection (2-way FSI)[mm]	Tip Deflection (1-way FSI)[mm]	Relative Difference [%]
10	20,82	19,59	5,89
15	47,95	45,82	4,44
20	88,58	81,13	8,42
25	142,59	127,32	10,71
30	204,88	182,89	10,73
35	269,29	250,38	7,02

B.3 Tip Twist

The next tables show the tip twist numerical results obtained by the simulations of the fin in all operating conditions. The results for the single iteration analysis, as well as the multiple iteration model are shown, along with the relative difference.

Table B.7: Tip Twist numerical results at 2º AoA

Speed [knots]	Tip Twist (2-way FSI)[mm]	Tip Twist (1-way FSI)[mm]	Relative Difference [%]
10	0,016	0,222	36,06
15	0,085	0,119	39,80
20	0,139	0,225	61,13
25	0,116	0,380	227,41
30	-0,012	0,521	4405,62
35	-0,266	0,861	422,98

Table B.8: Tip Twist numerical results at 4º AoA

Speed [knots]	Tip Twist (2-way FSI)[mm]	Tip Twist (1-way FSI)[mm]	Relative Difference [%]
10	0,101	0,114	12,68
15	0,228	0,303	32,67
20	0,369	0,538	42,64
25	0,466	0,895	91,89
30	0,460	1,395	203,225
35	-0,033	1,675	5185,39

Table B.9: Tip Twist numerical results at 6º AoA

Speed [knots]	Tip Twist (2-way FSI)[mm]	Tip Twist (1-way FSI)[mm]	Relative Difference [%]
10	0,194	0,208	7,65
15	0,441	0,482	9,41
20	0,692	0,872	25,98
25	0,845	1,320	56,23
30	0,809	1,833	126.30
35	0,528	2,466	366,40

B.4 Pressure Fields

This appendix contains the pressure fields for various sailing conditions, comparing the flow around the fin acting as a rigid body in a simple CFD simulation with the flow around the deformed fin after the multiple iteration FSI simulation. Flow fields with the same conditions are presented using the same scale in order to improve readability.

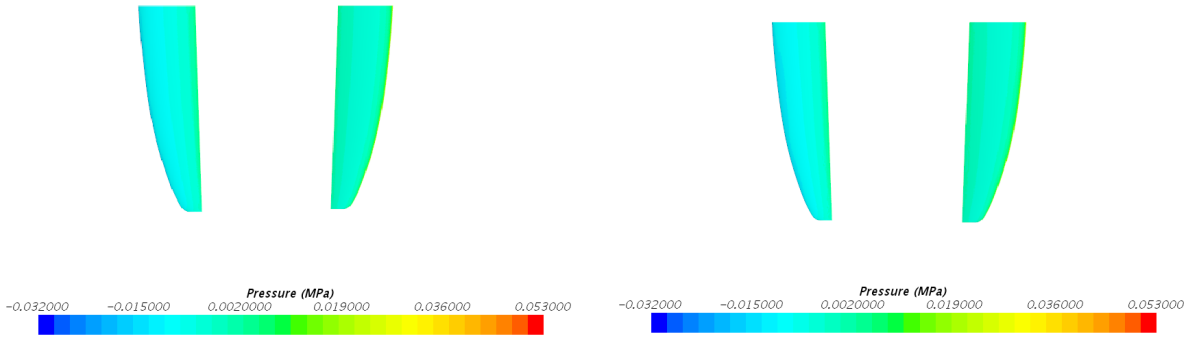

(a) Pressure field for rigid fin (V15 AoA2)

(b) Pressure field after two-way FSI (V15 AoA2)

Figure B.1: Pressure fields for 15 knots and 2º AoA

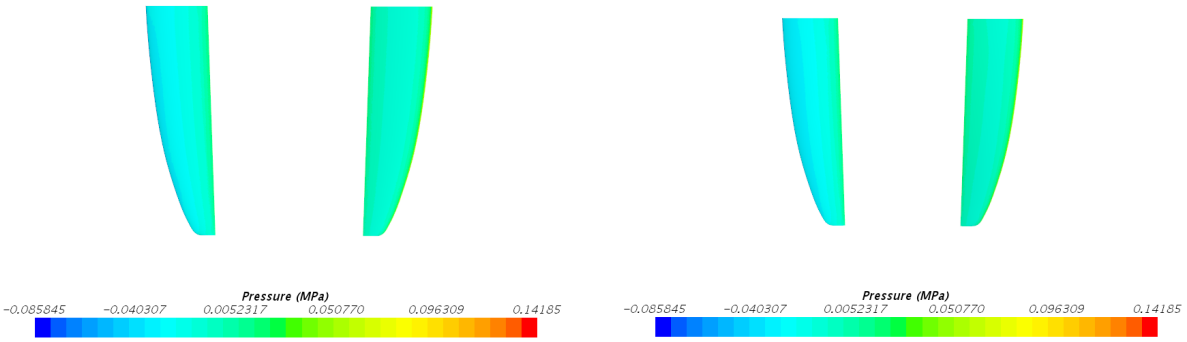

(a) Pressure field for rigid fin (V25 AoA2)

(b) Pressure field after two-way FSI (V25 AoA2)

Figure B.2: Pressure fields for 25 knots and 2º AoA

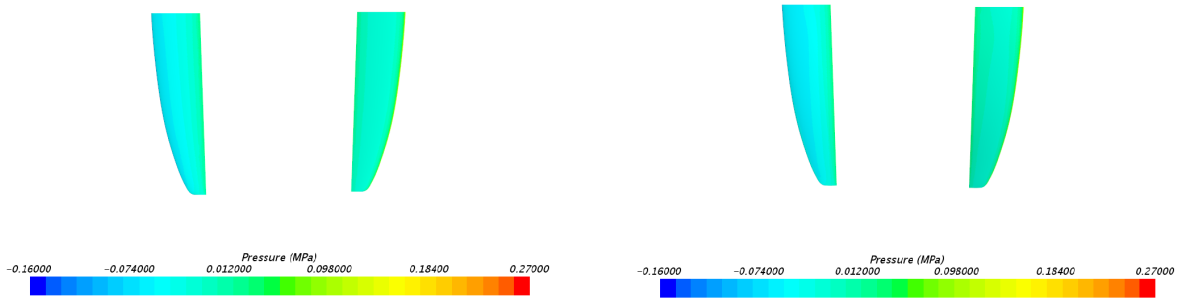

(a) Pressure field for rigid fin (V35 AoA2)

(b) Pressure field after two-way FSI (V35 AoA2)

Figure B.3: Pressure fields for 35 knots and 2º AoA

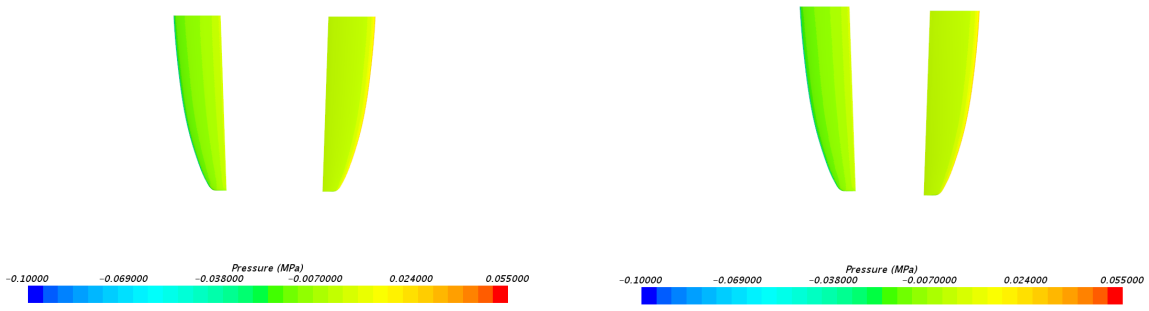

(a) Pressure field for rigid fin (V15 AoA4)

(b) Pressure field after two-way FSI (V15 AoA4)

Figure B.4: Pressure fields for 15 knots and 4º AoA

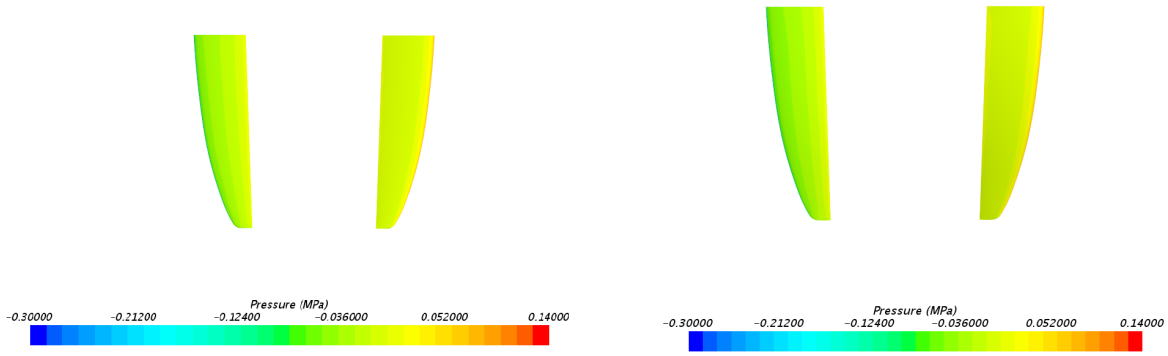

(a) Pressure field for rigid fin (V25 AoA4)

(b) Pressure field after two-way FSI (V25 AoA4)

Figure B.5: Pressure fields for 25 knots and 4º AoA

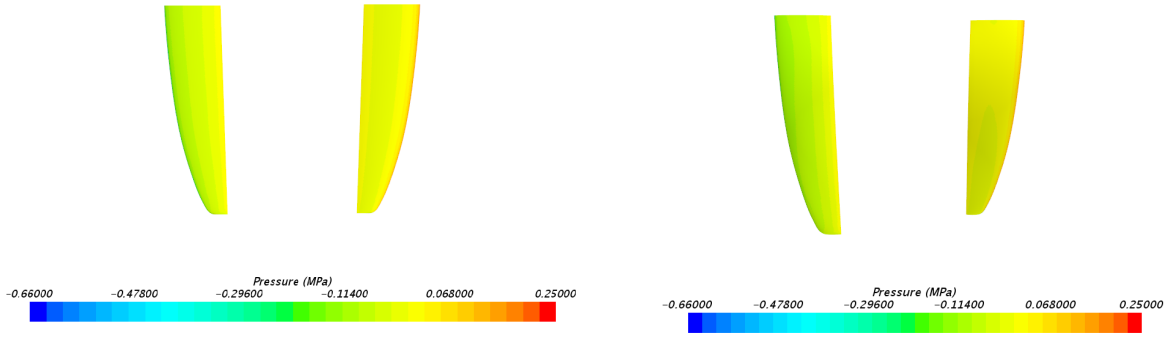

(a) Pressure field for rigid fin (V35 AoA4)

(b) Pressure field after two-way FSI (V35 AoA4)

Figure B.6: Pressure fields for 35 knots and 4º AoA

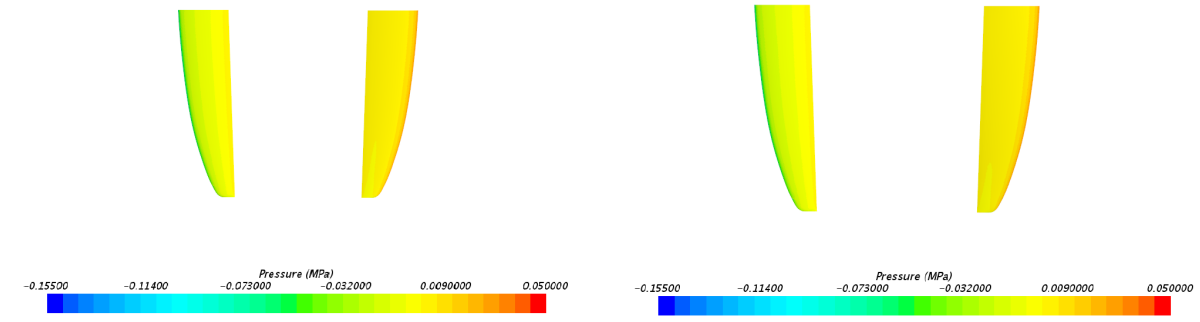

(a) Pressure field for rigid fin (V15 AoA6)

(b) Pressure field after two-way FSI (V15 AoA6)

Figure B.7: Pressure fields for 15 knots and 6º AoA

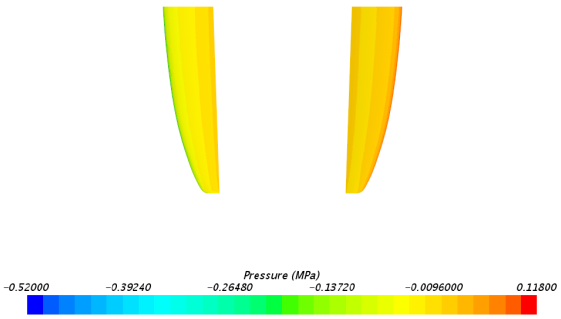

(a) Pressure field for rigid fin (V25 AoA6)

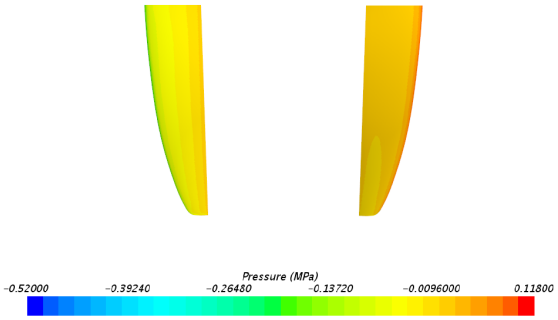

(b) Pressure field after two-way FSI (V25 AoA6)

Figure B.8: Pressure fields for 25 knots and 6º AoA

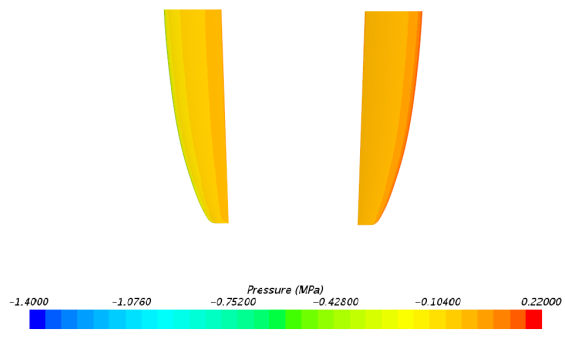

(a) Pressure field for rigid fin (V35 AoA6)

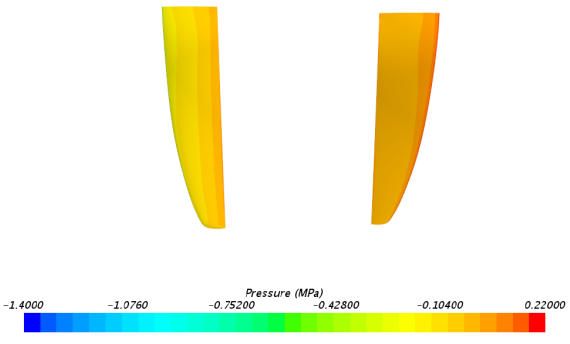

(b) Pressure field after two-way FSI (V35 AoA6)

Figure B.9: Pressure fields for 35 knots and 6º AoA